

1 **Function and three-dimensional structure of intervessel pit membranes in angiosperms: a**  
 2 **review**

3 Lucian Kaack<sup>1</sup>, Clemens M. Altaner<sup>2</sup>, Cora Carmesin<sup>1</sup>, Ana Diaz<sup>3</sup>, Mirko Holler<sup>3</sup>, Christine  
 4 Kranz<sup>4</sup>, Gregor Neusser<sup>4</sup>, Michal Odstreil<sup>3,5</sup>, H. Jochen Schenk<sup>6</sup>, Volker Schmidt<sup>7</sup>, Matthias  
 5 Weber<sup>7</sup>, Ya Zhang<sup>1,8</sup>, Steven Jansen<sup>1</sup>

6 Address details:

- 7 1. Institute of Systematic Botany and Ecology, Albert-Einstein-Alleen  
 8 11, Ulm University, D-89081 Ulm, Germany
- 9 2. New Zealand School of Forestry, University of Canterbury, Private Bag 4800,  
 10 Christchurch, New Zealand
- 11 3. Paul Scherrer Institut, Forschungsstrasse 111, 5232 Villigen PSI,  
 12 Switzerland
- 13 4. Institute of Analytical and Bioanalytical Chemistry, Albert-Einstein-  
 14 Alleen 11, Ulm University, D-89081 Ulm, Germany
- 15 5. Carl Zeiss SMT, Carl-Zeiss-Str. 22, 73447 Oberkochen, Germany
- 16 6. Department of Biological Science, California State University  
 17 Fullerton,  
 18 Fullerton, CA 92834-6850 U.S.A.
- 19 7. Institute of Stochastics, Helmholtzstr. 18, Ulm University, D-89069  
 20 Ulm, Germany
- 21 8. College of Life Sciences, Beijingdong Road 1, Anhui Normal University, 241000, China

*We dedicate this paper to Elisabeth Wheeler, Emmy van Nieuwkoop, and Pieter Baas for many years of support to wood anatomists worldwide.*

## **Abstract**

Pit membranes in bordered pits of tracheary elements of angiosperm xylem represent primary cell walls that undergo structural and chemical modifications, not only during cell death, but also during and after their role as safety valves for water transport between conduits. Cellulose microfibrils, which are typically grouped in aggregates with a diameter between 20 to 30 nm, make up their main component. While it is clear that pectins and hemi-cellulose are removed from immature pit membranes during hydrolysis, recent observations of amphiphilic lipids and proteins associated with pit membranes raise important questions about drought-induced embolism formation and spread via air-seeding from gas filled conduits. Indeed, mechanisms behind air-seeding remain poorly understood, which is due in part to little attention paid to the three-dimensional structure of pit membranes in earlier studies. Based on perfusion experiments and modelling, pore constrictions in fibrous pit membranes are estimated to be well below 50 nm, and typically smaller than 20 nm. Together with the low dynamic surface tensions of amphiphilic lipids at air-water interfaces in pit membranes, 5 to 20 nm pore constrictions are in line with the observed xylem water potentials values that generally induce spread of embolism. Moreover, pit membranes appear to show ideal porous medium properties for sap flow to promote hydraulic efficiency and safety due to their very high porosity (pore volume fraction), with highly interconnected, non-tortuous pore pathways, and the occurrence of multiple pore constrictions within a single pore. This three-dimensional view of pit membranes as mesoporous

media may explain the relationship between pit membrane thickness and embolism resistance, but is largely incompatible with earlier, two-dimensional views on air-seeding. It is hypothesised that pit membranes enable water transport under negative pressure by producing stable, surfactant coated nano-bubbles, while preventing the entry of large bubbles that would cause embolism.

Keywords: pit membrane, vessel, xylem, angiosperms, embolism, air-seeding, porous medium, ultrastructure

## Introduction

Bordered pits represent a key evolutionary anatomical xylem feature of vascular plants (Kenrick & Crane 1991; 1997). Indeed, the long-distance transport of water and nutrients, which is based on a transpiration-driven process that occurs largely under negative pressure, relies on openings in the secondary cell wall of water conducting xylem cells (vessels and tracheids). Since the  $< 2$  nm pores in secondary cell walls of conduits offer a very high hydraulic resistance (Donaldson et al. 2015, 2018), larger openings offered by bordered pits are highly important for efficient transport between conduits (Zimmermann & Brown 1971; Tyree & Sperry 1989; Choat et al. 2008). Although multicellular vessels with their perforation plates independently evolved in ferns s.l., Gnetales, and angiosperms (Thompson 1918; Bliss 1921; Muhammad & Sattler 1982; Carlquist & Schneider 2001; Pittermann et al. 2011), no vascular plant has been found yet, in which water is transported from the absorbing roots to transpiring leaves via a completely unsegmented system. Instead, water must pass through a highly redundant transport system by crossing hundreds to thousands of apoplastic connections, which are termed bordered pits because of the partly overarching shape of the secondary cell wall.

Although the ultrastructure and function of bordered pits has been described in many papers and textbooks (Schacht 1859; Choat et al. 2008), our understanding of the pit membrane ultrastructure remains far from complete. Based on empirical evidence, intervessel pit membranes account for about 50% of the hydraulic xylem resistivity (Choat et al. 2008), with the remaining hydraulic resistivity created by inner conduit walls and perforation plates between vessel elements (Ellerby & Ennos 1998; Sperry et al. 2005; Hacke et al. 2006; Christman & Sperry 2010). Besides creating hydraulic bottlenecks for sap flow, intervessel pit membranes are also involved in gas entry from embolised (gas-filled) vessels to water-filled ones, a process known as air-seeding (Zimmermann 1983; Sperry & Tyree 1988). While there is convincing evidence for air-seeding, our understanding of this process has been hampered by an overly simplistic and two-dimensional view of pit membrane structure that does not account for the three-dimensional structure of pores and the fibrous nature of pit membranes (Jansen et al. 2018). The long-standing question of how plants can transport water under negative pressure cannot be fully addressed without a solid grasp of the structure of conduit cell walls, pit membranes, and their functional implications for movement of water and gas. Recently, detailed anatomical observations at the nanoscale level, combined with both experimental and modelling approaches have opened up novel ways to investigate pit membranes as three-dimensional, porous media for xylem sap flow in plants.

This review aims to provide an overview of what is currently known about the development, chemical composition, and three-dimensional structure of intervessel pit membranes in angiosperm xylem. Since plant structure is closely tied to development, a short overview about the development of bordered pits in angiosperms is given. Special attention is paid to the three-dimensional structure of pit membranes, which is crucial for their functions with respect to

xylem sap flow. While vessel-tracheid and tracheid-tracheid pit membranes are important for xylem sap transport through tracheids (Pan & Tyree 2019), this review focusses on intervessel pit membranes only. We assume that bordered pit membranes between neighbouring tracheids and vessels of angiosperms are largely similar in structure and function (Liese & Côté, 1960), but vessels show higher hydraulic efficiency than tracheids (Zimmermann 1983). Gymnosperms, which have a very different pit membrane than angiosperms (Pittermann et al. 2005; Jansen & McAdam 2019), will not be discussed here. Moreover, a brief outlook on future research priorities is provided.

### **Bordered pit development**

Bordered pits are composed of overhanging secondary cell walls (the pit borders), which surround openings (the apertures) to the pit chambers on both sides of the centrally spanned and modified primary cell wall and middle lamella. The primary cell wall and middle lamella form the pit membrane (Fig. 1). While non-water conducting cells may also show distinct or indistinct pit borders, water conducting cells (vessel elements and tracheids) exclusively possess bordered pits (Sano et al. 2011). Bordered pits were long thought to develop in areas of the secondary wall where the primary wall was pierced by plasmodesmata, known as primary pit fields (Kerr & Bailey 1934; Wardrop 1958; Tschernitz & Sachs 1975; Juniper 1977), and that plasmodesmatal connections played a role in releasing hydrolytic enzymes for local targeted cell wall degradation and to prevent cellulose deposition (Juniper 1977). However, plasmodesmata are not essential for pit development and do not necessarily disrupt cellulose deposition (Barnett & Harris 1975; Barnett 1981, 1982). Absence of plasmodesmata from pit membranes is most common in pits of vessel elements and tracheids, while they are abundant in pit membranes between fibres,

parenchyma cells, and combinations of these cell types (Yang 1978; O'Brien 1981; Barnett 1982; Rabaey et al. 2008).

Ontogenetically, bordered pits are designated before secondary cell wall development by active ROP (Rho family guanosine triphosphatases of plants) proteins tethered to the specific locations of the plasma membrane. The initiated assembly of ROP11-MIDD1-Kinesin-13A complexes results in depolymerisation of cortical microtubules, preventing cellulose deposition by microtubule-guided cellulose synthases at these locations (Oda & Fukuda 2013; Bourdon et al. 2017; Sugiyama et al. 2017, 2019). Sites of bordered pits are initially marked out during early stages in the formation of the primary wall of tracheary elements as regions within the fusiform cambial cells that are free of cortical microtubules (Chaffey et al. 1997).

During secondary cell wall formation, circular bands of microtubules form around the pit apertures of bordered pits (Robards & Humpherson 1967; Uehara & Hogetsu 1993; Chaffey et al. 1997, 1999, 2000). These circular bands of cortical microtubules will then narrow centripetally, which results in a reduction of the pit aperture size as the bordered pit develops. When the cortical microtubules stop this constriction process, the pit aperture remains more or less constant, resulting in a pit canal. Upon completion of the bordered pit formation, the microtubules are disassembled. The circular bands of microtubules around the edges of developing pit borders are required for guiding the deposition of concentrically oriented cellulose microfibrils at pit borders via cellulase synthase (Chaffey et al. 2000; Funada 2000). The cellulose microfibrils in this area of the pit border, which represent an opening in the secondary wall, are deposited in a pattern that differs from the normal reticulate texture of the primary wall. The duration of the cell wall development and cambial differentiation of fusiform initials is under hormonal control, affected by environmental conditions, and phenology (Kitin & Funada

2016). While auxin concentrations are known to have an important effect on the development, dimensions, and arrangement of vessels (Johnson et al. 2018; Smetana et al. 2019), it is less clear how auxin may affect bordered pit development within a three-dimensional vessel network.

#### **The development and chemical composition of intervessel pit membranes**

The intervessel pit membrane is composed of the middle lamella and the primary cell walls of two adjacent vessels. During early developmental stages, before vessels become functional, the pit membrane, like any primary wall, is composed of pectins, cellulose, and hemi-cellulose, which cross-links cellulose microfibrils (Kim et al. 2012; Kim & Daniel 2013; Herbette et al. 2015; Sun et al. 2017) (Table 1).

During apoptosis (a highly regulated and controlled form of programmed cell death), hydrolytic enzymes remove most non-cellulosic compounds, including the cross-links, in a coordinated process, which might be associated with a swelling of the intervessel pit membrane and frequently results in a highly transparent, almost invisible pit membrane as viewed under a transmission electron microscope (Schmid & Machado 1968; O'Brien 1970; Kim et al. 2012; Kim & Daniel 2013; Klepsch et al. 2016; Buono et al. 2019) (Fig. 2). Some pectins remain in the annulus of the pit membrane (Schmid & Machado 1968; Jansen et al. 2009; Plavcová & Hacke 2011; Kim & Daniel 2013; Herbette et al. 2015; Schenk et al. 2018) and there is no evidence for pectins in the central parts of an intervessel pit membrane, making it unlikely that pit membranes change their thickness and porosity as a hydrogel due to ion mediated crosslinks between pectins (Zwieniecki et al. 2001; Plavcová & Hacke 2011; Nardini et al. 2011). It is unknown whether pectins remaining in the pit membrane annulus affect the mechanical properties of the actual pit membrane (Plavcová & Hacke 2011; Herbette et al. 2015). Moreover, pectins remain present in the protective layer and possibly the pit membrane of vessel-parenchyma pits. The extracellular

peptide Kratos was recently found to protect vessel-associated parenchyma cells in *Arabidopsis* from cell death by hydrolytic enzymes. These Kratos peptides are missing between intervessel pit membranes (Escamez et al. 2019), which explains the lack of pectins in intervessel pit membranes and their presence in vessel-parenchyma pits. The up-regulation of protease genes in various species could only partially reveal details of the mechanics, subcellular localisation, and target identification of proteases during apoptosis of tracheary elements. Identified hydrolytic enzymes in transdifferentiating mesophyll cells in the in-vitro system of *Zinnia elegans* (Asteraceae) include Zinnia endonuclease1 (ZEN1), and various proteases, such as cysteine and serine proteases, and thrombin-like protease (TLP), which could be involved in maturation of pit membranes (Ito & Fukuda 2002; Iakimova & Woltering 2017).

While hemi-cellulose cross-links are absent in pit membranes (Herbette et al. 2015), there are some records of weak signals for lignin in pit membranes (Table 1). Traditional staining for lignin with safranin and fast green (Bamber 1961) combined with autofluorescence studies find little evidence for lignin in pit membranes (Schenk et al. 2018), but some immunolabeling studies found small amounts of lignin in *Populus tremula* x *P. alba* (Salicaceae) (Herbette et al. 2015) and metaxylem of *Arabidopsis* (Brassicaceae) (Ruel et al. 2012). Small amounts of lignin were also suggested to occur in intervessel pit membranes of *Rhizophora mucronata* (Rhizophoraceae) and *Avicennia marina* (Acanthaceae) (Schmitz et al. 2007), as well as *Populus nigra* (Salicaceae) (Pereira et al. 2018). However, contamination during sample storage and/or preparation, as well as accumulation of lignin traces and other phenolic extractives carried with the xylem sap, could have affected lignin observations in these studies.

Fully developed pit membranes are mainly composed of cellulose, but also include all the components found in xylem sap, such as ions, carbohydrates, peptides, proteins, and lipids.



1 Proteins were detected in pit membranes of several angiosperm species based on staining with  
 2 NanoOrange (Neumann et al. 2010; Schenk et al. 2018). Evidence for the presence of  
 3 amphiphilic, insoluble lipids associated with the inner walls of water conducting cells, pit  
 4 borders, and pit membranes is based on staining with FM1-43, which is an excellent dye for  
 5 lipids, including amphiphilic lipids and biological membranes (Fig. 2), and post-fixation of  
 6 samples for transmission electron microscopy (TEM) with OsO<sub>4</sub> (Schenk et al. 2017, 2018;  
 7 Jansen et al. 2018) (Fig. 3). Pit membranes in TEM samples that are only treated with uranyl  
 8 acetate and lead citrate and not with OsO<sub>4</sub> are hardly visible due to their transparency, while  
 9 OsO<sub>4</sub> makes them more electron dense. OsO<sub>4</sub> is known to bind to double carbon bonds of  
 10 unsaturated fatty acid chains of lipids, some proteins and lipoprotein complexes (Riemersma  
 11 1968). Recent analyses of xylem sap based on mass spectrometry provide direct evidence for the  
 12 presence of phospholipids and galactolipids (Schenk et al. 2019). Imaging via confocal  
 13 microscopy with FM1-43 shows distinct lipid layers on both sides of pit membranes, but not in  
 14 their interior (Fig. 2), while transmission electron microscopy shows lipids inside membranes in  
 15 addition to outside layers (Schenk et al. 2018) (Fig. 3) It is unclear whether the difference  
 16 between the two types of microscopy is due to relocation of lipids into the pit membrane by the  
 17 organic solvents used during TEM preparation, or if the FM1-43 cannot penetrate through lipid  
 18 layers into the actual pit membrane. Importantly, a non-microfibrillar, interstitial coating was  
 19 found on dried and fresh pit membranes of *Triadica sebifera* (Euphorbiaceae), *Laurus nobilis*  
 20 (Lauraceae), and *Nicotiana tabacum* (Solanaceae) observed via atomic force microscopy (AFM)  
 21 (Pesacrete et al. 2005; Nardini et al. 2011; Lee et al. 2012). Since this layer had a thickness of 2  
 22 to 5 nm and was very sensitive to perturbation by the AFM tip, it is quite possible that this  
 23 coating layer consists of the lipids observed under confocal microscopy based on staining with

FM1-43. Moreover, some pit membranes from overwintering vessels and heartwood of *T. sebifera* were found to be covered by a very heavy, encrusted layer (Pesacreta et al. 2005). The deposition of a coating layer on intervessel pit membranes has also been observed in *Fraxinus americana* (Oleaceae) during winter, with subsequent removal of this layer in spring (Wheeler 1981). Seasonal variation in the chemical composition of pit membranes is suggested by high transparency of young, freshly developed intervessel pit membranes, while older pit membranes are typically more electron dense (Schmid & Machado 1968). It is, however, unclear whether this change in electron density indicates that apoplastic lipids are released from vessel-associated parenchyma cells into vessels and tracheids.

Unlike intervessel pit membranes, the entire primary wall at perforation sites between adjacent vessel elements is completely hydrolysed (Yata et al. 1970). How exactly the microfibrillar network is removed at perforation sites is unclear (Meylan & Butterfield 1981; Butterfield 1995). It can be suggested that differences in cell wall chemistry during early developmental stages could explain the entire removal of the primary wall at the perforation plate, which is mainly composed of pectins, includes almost no cellulose, and does not become lignified (Benayoun et al. 1981; Chaffey et al. 1999) (Fig. 2). For example, microtubules seen at the periphery of the perforation plate of vessel elements in hybrid aspen (*Populus tremula* L. x *P. tremuloides* Michx.) are thought to guide enzyme-containing vesicles to the perforation plate. There, the vesicles filled with enzymes are trapped by the microfibrils that overlay the actual perforation plate, and the enzymes are locally released in a coordinated process (Chaffey et al. 2002). Although there is some analogy between the development of bordered pits and perforation plates, pit membranes do not dissolve completely, as discussed above.

### **Intervessel pit membrane thickness**

Angiosperm pit membranes are composed of a mesh of cellulose microfibril aggregates, which frequently form thicker aggregates. The microfibril aggregates are arranged randomly, forming a non-interwoven meshwork, with microfibril aggregates spanning the entire pit membrane and continuing into the pit membrane annulus and primary cell wall. The thickness of intervessel pit membranes shows considerable variation, with values from below 200 nm to more than 1,000 nm (Jansen et al. 2009). Pit membrane thickness was found to be a major determinant of embolism resistance, with thick ( $> 500$  nm) pit membranes characterising drought resistant species with relatively high embolism resistance, while thin (200 to 300 nm) pit membranes typically found in temperate species exhibiting lower embolism resistance (Lens et al. 2011; Scholz et al. 2013; Li et al. 2016; Jansen et al. 2018). It is recently discussed whether potential differences in pit membrane thickness between organs and between vessels of different sizes can also be linked to possible changes in embolism resistance (Klepsch et al. 2018, Pfautsch et al. 2018, Dória et al. 2019, Kotowska et al. 2019). The correlation between pit membrane thickness and embolism resistance was initially hypothesized to be caused by thick pit membranes having more narrow pores than thin pit membranes, and possibly by considerable differences in mechanical properties, especially those affecting aspiration and stretching of the pit membrane towards the pit border (Choat et al. 2004; Jansen et al. 2009). Possible differences in effective pore sizes between membranes of different thickness are discussed below when considering their three-dimensional structure.

Pit membranes of angiosperms are generally described as having an evenly thick pit membrane, unlike the torus-margo structure of gymnosperms (Liese 2007; Bouche et al. 2014). Some angiosperms, however, are characterised by a clear, central thickening, which is typically slightly larger than the outer pit aperture and has been referred to as a torus. Examples include

1 Cannabaceae (*Celtis*), Oleaceae (*Chionanthus*, *Osmanthus*, *Picconia*), Rosaceae (*Cercocarpus*),  
 2 Schisandraceae (*Schisandra*), Thymelaeaceae (*Daphne*, *Wikstroemia*), and Ulmaceae (*Ulmus*,  
 3 *Planera*, *Zelkova*) (Wheeler 1983; Jansen et al. 2007, 2010; Dute et al. 2010, 2011; Sano et al.  
 4 2013). These torus-bearing pit membranes are found in intervessel pits, but limited to tracheid-  
 5 tracheid pit membranes in various species. Importantly, the occurrence of a torus is associated  
 6 with a circular to oval shape of the outer pit aperture.

7 The thickness of pit membranes is not fixed, and typically undergoes considerable changes  
 8 during its lifetime. After hydrolytic enzymes have removed the non-cellulosic compounds, a  
 9 slight swelling of pit membranes has been noticed (Schmid & Machado 1968) (Fig. 2), most  
 10 likely due to the removal of hemicellulose cross-links between microfibrils. During dehydration,  
 11 however, pit membranes may shrink by ca. 50% (Zhang et al. 2017, 2019; Kotowska et al. 2019).  
 12 Shrinkage may also occur by mechanical deformation or mechanical pressure differences across  
 13 the pit border (Tixier et al. 2014). Pit membrane shrinkage is associated with aspiration, and  
 14 becomes more common in xylem of older growth rings (Kotowska et al. 2019). Pit membranes  
 15 were found to have strongly reduced permeability after drying due to partial or complete  
 16 blockage of pit membrane pores in *Eucalyptus* (Rudman 1966; Kininmonth 1971, 1972). More  
 17 recent studies have found that pit membrane shrinkage due to dehydration is associated with a  
 18 strong reduction of pore constrictions and porosity, as well as an increase in the geodesic  
 19 tortuosity and constrictivity of pores (Zhang et al. 2019). Shrinkage of pit membranes and  
 20 deposition of phenolic substances on pit membranes is associated with heartwood formation  
 21 (Kininmonth 1972). The occurrence of reduced pore sizes in shrunken, dried pit membranes  
 22 should make these less prone to air-seeding, not more, as predicted based on air-seeding fatigue  
 23 (also termed cavitation fatigue) (Hacke et al. 2001; Hillabrand et al. 2016). Air-seeding fatigue

describes an increase of xylem vulnerability after an embolism-refilling cycle of the same xylem sample. Since air-seeding fatigue has only been found for species of *Aesculus*, *Helianthus*, and *Populus* (Hacke et al. 2001, Stiller & Sperry 2002), which are characterised by very thin pit membranes, it may be limited to species with thin pit membranes that easily develop large pores after dehydration (Zhang et al. 2017).

### **Three-dimensional characterisation of pit membranes as porous media**

Surprisingly, the three-dimensional porous medium characteristics of pit membranes have only recently been modelled (Zhang et al. 2019). In that model, pit membranes were composed of several layers or stacks of cellulose microfibril aggregates, with equal distance between each layer. The number of layers depended on the thickness of the pit membrane. Between 6 and 8 layers were found to occur in five temperate forest tree species, while *Persea americana* (Lauraceae) and *Cinnamomum camphora* (Lauraceae) had 12 and 18 layers, respectively (Zhang et al. 2019). The model assumed that completely dried, fully shrunken pit membranes have zero distance between each layer, and zero distance between two or three randomly grouped microfibril aggregates within a layer. While these assumptions were fairly realistic, further improvement of this three-dimensional model should account for random orientation of cellulose microfibril aggregates within a layer, with a non-homogeneous distribution of pore spaces.

Based on our current understanding, the porosity or pore volume fraction of fresh pit membranes is very high (ca. 81%), as expected for natural, fibrous porous media (Vallabh et al. 2010, 2011; Shou et al. 2011). Geodesic tortuosity values (ratio of the mean shortest flow path length to the thickness of the porous medium) (Peyrega & Jeulin 2013, Neumann et al. 2019) were very low (ca. 1.03), and indicate that water molecules pass pit membranes along a non-tortuous pathway that is barely longer than the actual thickness of pit membranes. Therefore, pit membranes are

mainly composed of effective pores, which are highly interconnected, without a tortuous or zigzagging pathway, despite their irregular pore shapes and volumes (Fig. 4). Pores between cellulose microfibril aggregates within the same layer are typically slit- or V-shaped, and not circular or oval as often assumed in previous models of pit membrane pores (Schenk et al. 2015). Pore spaces within a single pore path vary in their volume, with pore constrictions acting as hydraulic bottlenecks between larger pore spaces. From a mathematical point of view, constrictivity ( $\beta$ ) is defined as:

$$\beta = (R_{\min} / R_{\max})^2.$$

$R_{\max}$  is the maximum radius of (overlapping) spheres that would cover at least 50% of the pore space in a porous medium, and  $R_{\min}$  is the maximum radius of spheres that could theoretically move through the pore constrictions in a certain direction to cover at least 50% of the pore space. While the constrictivity of a pore consisting of a perfectly straight, tube-like opening without any constriction (Fig. 4) equals 1, a lower constrictivity value of 0.76 for pit membranes indicates that constrictions occur (Zhang et al. 2019). These constrictions or pore throats represent the hydraulic bottlenecks in pit membranes. So far, three-dimensional porous medium characteristics of pit membranes are obtained by modelling, and have not been measured directly based pit membrane images.

### **The concept of pore constriction in pit membrane pores**

Sizes of pit membrane pores have been reported in various studies, including many on the permeability of preservatives in both fresh and dried wood (Rudman 1966; Kininmonth 1971, 1972; Choat et al. 2003; Williamson & Milburn 2017). While the term pit membrane pore size is frequently used in literature, it does not clearly relate to the three-dimensional structure of the entire pore pathway, with pores consisting of several to many pore constrictions, depending on

1 pit membrane thickness. Thin pit membranes are likely to have pores with 5 to 10 constrictions,  
2 while thick pit membranes include pores with 10 to more than 20 variously-sized constrictions  
3 (Fig. 4). To highlight the three-dimensional structure of pit membranes and refer to hydraulic  
4 bottlenecks explicitly, we suggest using the term pore constriction or constriction size instead of  
5 pore size. Pore constrictions are hydraulically the most important structures, with the smallest  
6 pore constriction being most crucial for flow across a pit membrane as well as for air-seeding.

7 Experiments based on electron microscopy and perfusion experiments with a wide range of  
8 solutions, such as India ink, paint particles, heavy metal salt solutions, and colloidal gold  
9 particles have found that pit membrane pore constrictions are clearly larger than the pores in  
10 vessel cell walls, and therefore the most important apoplastic pathway for sap flow between  
11 water conducting cells (Rudman 1966; Kininmonth 1971, 1972; Murmanis & Chudnoff 1979).

12 Experiments with different sizes of colloidal gold particles suggest that maximum pore  
13 constrictions in fresh (never-dried) pit membranes are well below 50 nm, most commonly around  
14 5 to 20 nm (Choat et al. 2003, 2004; Zhang et al. 2017, 2019). A similar estimation of pore  
15 constrictions around 23 nm was found based on a shrinkage model, which considered the  
16 difference in pit membrane thickness between fresh and fully dehydrated pit membranes (Zhang  
17 et al. 2017, 2019). These values are much smaller than the >100 nm sizes that have been  
18 observed via scanning electron microscopy (Shane et al. 2000; Sano 2005; Jansen et al. 2008,  
19 2009; Hillabrand et al. 2016) and older estimations based on air-seeding pressures (Jansen et al.  
20 2009). The main explanation for this discrepancy is that dehydration and/or chemical treatment  
21 during sample preparation appear to cause artificial enlargement of pore constrictions, especially  
22 in species with thin pit membranes. According to a frequently cited hypothesis, a rare wide pore  
23 may exist in one of the hundreds to thousands of pit membranes that interconnect neighbouring

vessels, and this rare pore may cause air-seeding and hydraulic failure (Wheeler et al. 2005; Plavcová et al. 2013). This “rare pit hypothesis” (or pit area hypothesis, because a larger pit area would have a higher probability of containing a large pore) cannot be tested in any direct approach, because it is extremely difficult to locate the largest pore in all pit membranes of an entire vessel. The hypothesis is also based on problematic assumptions, because both the scanning electron microscope used to detect such large pores and hydraulic methods to test the hypothesis are affected by experimental artefacts (Jansen et al. 2015). Moreover, the rare pit hypothesis is based on a rather simplistic, two dimensional view of a pit membrane. As mentioned above, a single pore contains 4 to more than 20 pore constrictions, and the likelihood that all pore constrictions are extremely large becomes very low with increasing pit membrane thickness. Since thick pit membranes encompass a higher amount of pore constrictions, chances that the narrowest pore constriction within a long pore is wider than 50 nm are strongly reduced. Increased embolism resistance could also be expected for torus-bearing angiosperm species, although this has not been systematically tested.

Direct imaging of pit membrane pore spaces in fully hydrated pit membranes would be ideal to reveal the true 3D structure of pore spaces, but imaging of hydrated cellulose is technically highly challenging (Xu et al. 2006; Reza et al. 2015; Kaushik et al. 2015; Rongpipi et al. 2018). Moreover, the penetration capacity of colloidal gold particles into pit membranes does not provide a pore constriction distribution. Penetration of gold particles could be affected by their hydrophobic nature, which may also become coated by amphiphilic lipids in xylem sap (Schenk et al. 2017, 2018; Zhang et al. 2019). Additional factors that may affect the permeability of pit membranes to gold particles or other substances include electroviscosity and boundary layers around the hydrophilic cellulose microfibrils (Santiago et al. 2013; Sulbarán et al. 2014).



Nevertheless, these limitations would lead to measuring errors within a nm range only. If these effects cause a slight underestimation of pore constrictions, they are still unlikely to underestimate sizes by a factor of 5 to 10 times, which would be required to result in pore sizes seen under scanning electron microscopy. Nanoscale adsorption-induced deformation of pit membranes could be discussed in the manner of keeping cellulose fibrils in place to maintain the pore constrictions. Adsorption-induced deformation is a well-known process in nanoporous media and describes swelling (expansion) and shrinkage (contraction) of the media, due to interaction of the high surface area of the solid component (adsorbent) with molecules of the fluid (adsorbate) whereas the molecules of the fluid can dynamically attract or repel each other (Gor et al. 2017).

### **Hydraulic resistance of pit membranes**

The mesoporous (5-50 nm) mesh of pit membranes appears to be essential for preventing the spread of embolism and maintaining the integrity of the xylem sap transport system. However, the small pore constrictions of pit membranes also add hydraulic resistance to the xylem pathway. For many years, it has been well known that the measured hydraulic resistance of the xylem is higher than that based on calculations from the Hagen-Poiseuille equation using the conduit diameters measured in cross sections of wood (Ewart 1906; Zimmermann & Brown 1971). The additional resistance was thought to come from the transfer resistance of water across pit membranes of vessels and tracheids. Indeed, water moving through xylem conduits encounters three principal resistances: (1) the resistance due to friction along conduit walls, (2) the resistance due to pit membranes as water crosses from one conduit into the next, and (3) the resistance caused by perforation plates between vessel elements.

In modelling approaches, the resistance of pit membranes has been calculated as a thin porous plate, where resistance scales with the 3<sup>rd</sup> power of the average membrane pore diameter (Sperry & Hacke 2004). Not surprisingly, however, mathematical modelling has generally proven unsatisfactory and underestimated resistance of pit membranes because of a two dimensional approach that considers pores to be cylindrical (Sperry & Hacke 2004; Wheeler et al. 2005).

Empirical estimates of pit resistance have mainly been acquired by a subtraction method, whereby the theoretical resistance calculated from the conduit diameters is subtracted from the total measured resistance of a stem or root, with the remaining amount of resistance considered to be pit membrane resistance (Sperry et al. 2005; Hacke et al. 2006). These measurements indicated that pit membrane resistance, which is normalised to the pit membrane surface area for comparison between species, varied widely across species ranging from 0.14 to around  $2.00 \times 10^3 \text{ MPa s m}^{-1}$ . Schulte & Gibson (1988) used a different approach and estimated pit membrane resistance by measurements before and after pit membranes were dissolved using cellulase. These measurements, carried out on stems and petioles of three angiosperm species, gave relatively low values of pit membrane resistivity between 1.04 and  $2.86 \text{ MPa s m}^{-1}$ . Direct measurement of pit resistance across a single connection between two vessels resulted in higher values of the area specific resistance of pit membranes ( $2.56 \times 10^3$  to  $5.32 \times 10^3 \text{ MPa s m}^{-1}$ ) for two ring-porous tree species (Choat et al. 2006). Averaged across 60 species, the contribution of pit membrane resistance to total xylem hydraulic resistance is estimated to be 58% (Choat et al. 2008), with values ranging from 14 to 89% of the total xylem hydraulic resistance (Schulte & Gibson 1988; Sperry et al. 2005; Pittermann et al. 2005; Choat et al. 2006; Hacke et al. 2006). Interestingly, there is a trend of increasing pit membrane resistance with increasing conduit wall resistance (Sperry et al. 2005). It is unclear to what extent the estimated pit membrane resistance

values represent differences in pit membrane thickness or sizes of pore constrictions. Besides pit membrane resistance, hydraulic resistance at the bordered pit level may be affected by the pit aperture fraction (pit aperture area per pit membrane area), and the pit-field fraction (fraction of intervessel wall surface occupied by intervessel pits). All studies mentioned above do not account for the resistance provided by different types of perforation plates. Christman & Sperry (2010), for instance, showed that scalariform perforations can double lumen flow resistance.

### **Pit membranes and air-seeding**

There is some disagreement about how embolisms form *de novo* in fully functional xylem (Choat et al. 2016), but there is strong and convincing evidence that once a drought-induced embolism has formed, it spreads through pit membranes into adjacent conduits via a process known as air-seeding (Zimmermann 1983; Sperry & Tyree 1988). For this reason, embolism spreading during drought typically follows patterns of vessel connectivity (Brodersen et al. 2013; Choat et al. 2016; Brodribb et al. 2016, Roth-Nebelsick 2019). The air-seeding process is strongly affected by the pore geometry in pit membranes (Schenk et al. 2015), and, as discussed above, the pathway for xylem sap transport and spreading of gas from one vessel to another is a relatively straight path consisting of a series of variable pore spaces with multiple pore constrictions.

Air-seeding, as described in many papers and textbooks, is generally said to be determined by the “largest pore” in a pit membrane. This reasoning, however, is incorrect and based on a two dimensional view of pit membranes, with an unrealistic concept of what pit membrane pores are like (Jansen et al. 2018; Zhang et al. 2019). Air-seeding through a pore constriction of any shape can be quantified based on a modified Young-Laplace equation (Fig. 5) by,

$$\Delta P = \kappa \frac{2 \gamma \cos(\alpha)}{R},$$

where  $\Delta P$  is the pressure required to induce air-seeding (the pressure difference between the gas, including water vapour, and the xylem sap pressure),  $\kappa$  is a dimensionless shape correction factor between 0 and 1 (Schenk et al. 2015),  $\gamma$  is the surface tension of xylem sap,  $\alpha$  is the contact angle of the gas-xylem sap interface with the solid cellulose microfibril, and  $R$  is the smallest pore constriction radius. While  $\alpha$  is typically assumed to be zero because the meniscus is in contact with water absorbed onto cellulose of microfibril aggregates (Schenk et al. 2015), it is incorrect to assume that  $\gamma$  represents the relatively high surface tension of pure water of 72 mN / m (Christensen-Dalsgaard et al. 2011; Schenk et al. 2015, 2017, 2018). The presence of films of insoluble, amphiphilic lipids at air-water interfaces in pit membranes depends on the local lipid concentration per film surface area, which is known as the concept of dynamic surface tension and is very different from the under saturated surface tension of bulk xylem sap with very low concentrations of lipids (Schenk et al. 2017). The equilibrium surface tension of lipids extracted from xylem sap would be around 25 mN / m (Schenk et al. 2018).  $R$  represents the diameter of the smallest pore constriction within the shortest and widest pore pathway through a pit membrane, because that constriction will determine how much pressure difference it takes to force a gas bubble into the sap.

In Fig. 5, the pore constriction diameter is plotted as a function of air-seeding pressure, assuming a contact angle  $\alpha$  of zero, a shape correction factor  $\kappa$  of 0.5 (Meyra et al. 2007; Schenk et al. 2015, 2017), and two different values for the surface tension  $\gamma$  (25 mN / m for the dynamic, equilibrium surface tension of xylem sap lipids, and 72 mN / m for pure water). For a surface tension of 25 mN / m, air-seeding at 1 and 2 MPa pressure difference is calculated to occur at a pore constriction diameter of 50 and 25 nm, respectively, which is realistic with observed pore constrictions in pit membranes and measurements of embolism in xylem vulnerability curves

(Choat et al. 2012). A median  $\Psi_{12}$  value, which represents the xylem water potential  $\Psi$  corresponding to 12% loss of maximum hydraulic conductivity, was found to be -1 MPa (interquartile range: 1.6,  $x_L$ : -2 MPa,  $x_U$ : -0.4 MPa,  $n = 143$ ) based on 143 angiosperm species (Bartlett et al. 2016). A surface tension of 72 mN /m, however, would require pore constriction diameters of 144 nm and 72 nm for air-seeding at 1 and 2 MPa, respectively, much larger than the pore constrictions of 20 nm actually observed in fully hydrated pit membranes. Without a pore shape correction factor ( $\kappa = 1$ ), pore constrictions required for air-seeding would even double in diameter. Therefore, the presence of amphiphilic lipids associated with pit membranes will have strong effects on the surface tension at the site of air-seeding, and low surface tension is actually required to explain the spread of embolism through the tiny membrane pores. Thus, lipid layers on pit membranes do not provide a major challenge to the cohesion-tension theory, which is based on the high surface tension of water not in xylem, but in leaf cell walls, where water evaporates into air spaces inside the leaf (Askenasy 1895; Dixon & Joly 1895; Dixon 1914).

In addition to the sizes of pore constrictions, changes in pore space volumes play an additional role in air-seeding because bubble snap-off events and Haines Jumps of gas-water interfaces will occur if the radius of the constriction is less than half the radii of the pore volumes on either side of the constriction (Schenk et al. 2015; Park et al. 2019). Clearly, thick pit membranes have more pore constrictions than thin pit membranes, due to a higher number of cellulose layers (Fig. 4). Assuming a Poisson distribution, the smallest constriction size of each effective pore decreases with pit membrane thickness, which would explain the increased hydraulic safety of thicker pit membranes (Li et al. 2016). The exact mechanism of nanobubble formation by snap-off events, however, remains unclear, and it is also unknown to what extent pore volumes may change under

local pressure differences, to what extent microfibril aggregates could bend or re-arrange during this process, and what role lipids play in the process. Expansion of lipid coated nanobubbles under negative pressure conditions is theoretically inhibited by dynamic changes in the surface tension, which are caused by stretching the limited amount of lipid molecules of the coat. Moreover, coated nanobubbles are stable below a critical size threshold as long as expansion pressure is in equilibrium with the Laplace pressure. A sudden increase in surface tension due to fracture of the lipid coat causes an increase in Laplace pressure, which would compress and dissolve the nanobubble (Schenk et al. 2015, 2017). Therefore, air-seeding can create stable, coated nanobubbles, and bubble formation under negative pressure does not automatically result in embolism, which is supported by the observation of surfactant coated nanobubbles in xylem sap based on freeze-fracture TEM (Schenk et al. 2017). Further work is needed to investigate how exactly pit membranes may function as foam-producing structures, generating surfactant coated bubbles (Jansen et al. 2018).

#### **Mechanical properties and aspiration of pit membranes**

There are only a few studies on the mechanical properties and aspiration of angiosperm pit membranes. Based on nanoindentation measurements using atomic force microscopy to study the stiffness of the intervessel pit membrane, a Young's modulus of 0.4 GPa was found for *Populus deltoides* x *P. nigra* (Salicaceae) (Capron et al. 2014). Similar Young's moduli were found for both a dried and a rewetted pit membrane. However, irreversible shrinkage of dehydrated pit membranes (Hillabrand et al. 2016; Li et al. 2016; Zhang et al. 2017, 2019; Kotowska et al. 2019) due to the formation of hydrogen bonds between the hydroxyl groups of cellulose fibrils (Kroon-Batenburg et al. 1986; Hillabrand et al. 2016; Martínez-Sanz et al. 2017) does not allow us to make final statements about potential differences between the Young's

moduli of wet, fully hydrated pit membranes in their native state and in dry state. The cellulosic nature of pit membranes also results in a relatively low electric potential, with cellulose microfibrils and larger aggregates being slightly negatively charged, causing swelling by electrostatic repulsion and the hydrophilic nature of the fibres (Lindström et al. 2005; Fardim et al. 2005; Weber et al. 2013; Zhang et al. 2016). Moreover, charged structures would generate an electro-viscous effect that would increase hydraulic resistance of the pit membrane pore constrictions (van Doorn et al. 2011; Santiago et al. 2013). During dehydration, however, when water is removed from the pit membrane, these electrostatic forces are overcome by strong hydrogen bonds, which may also explain the irreversible nature of pit membrane shrinkage. It is therefore likely that the mechanical properties differ between fresh and rewetted pit membranes. The irreversibility of pit membrane shrinkage could explain air-seeding fatigue in species with very thin pit membranes due to irreversible formation of large pores (Hacke et al. 2001; Jansen et al. 2018, Zhang et al. 2017).

Whether air-seeding happens before or after aspiration remains unclear and requires experimental verification. Conceptually, however, air-seeding requires gas on one side of the membrane and sap under negative pressure on the other, so it is difficult to conceive of a scenario where air-seeding would occur through a non-aspirated membrane (Petty & Preston 1972; Sperry & Hacke 2004; Tixier et al. 2014). Additionally, morphological parameters such as shallower pit chambers, smaller apertures together with thicker pit membranes seem to increase hydraulic safety (Lens et al. 2011), indirectly supporting the assumption of air-seeding occurring after pit membrane aspiration. Once the pressure difference is overcoming the critical air-seeding pressure, the air-water meniscus travels through the pit membrane pore spaces and either produces a series of snap-off nanobubbles (Schenk et al. 2015; Park et al. 2019), or results in

continuous gas flow until the neighbouring vessel embolises (Zimmermann 1983; Sperry & Tyree 1988; Sperry & Hacke 2004; Choat et al. 2004; Lens et al. 2011).

### Questions for future research

Several important questions about pit membranes and their functional implications for xylem sap in plants remain unresolved. Here, we identify three future research areas of relevance. Firstly, from a structural point of view, more detailed ultrastructural observations of pit membranes and 3D imaging will be needed to develop a realistic, 3D model. Such a model could then be implemented in two-phase and multi-phase 3D flow simulations, and could even be combined with 3D reconstructions of bordered pits (Fig. 1) and entire vessel networks. Major challenges for developing such models include observations of fully hydrated pit membranes in their native state without preparation artefacts and differentiation of the pore spaces vs. cellulose fibrillar aggregates (Xu et al. 2006; Reza et al. 2015; Kaushik et al. 2015; Buesch et al. 2016; Rongpipi et al. 2018; Osorio et al. 2018). A combination of electron microscopy, X-ray nano-imaging, and other approaches, such as atomic force microscopy and super-resolution confocal microscopy, might be useful. Ptychographic x-ray scattering computed tomography at cryogenic conditions (cryo-PXCT) (Fig. 1), for instance, provides a fast way to obtain 3D reconstructions with a potential resolution below 30 nm of relatively large samples (ca. 50  $\mu\text{m}^3$ ) compared to the sample sizes for (S)TEM tomography (scanning transmission electron microscopy tomography) and destructive FIB-SEM tomography (focused ion beam - scanning electron microscopy) (Shahmoradian et al. 2017, Holler et al. 2018). By using cryogenic conditions, high resolution 3D reconstructions of bordered pits and pit membranes in a nearly natural and hydrated state with reduced radiation damage are feasible. Micro CT, an x-ray approach often used on plant



material to track embolism in xylem shows resolutions in the range of 2-6  $\mu\text{m}$  (Choat et al. 2016; Skelton et al. 2017).

A second major challenge is determining the mechanisms of air-seeding including lipid coated nanobubble formation behaviour, which may well represent one of the most important shortcomings in our understanding of xylem sap transport under negative pressure. Engineered devices that possess nanocapillaries from which water evaporates, referred to as “synthetic trees”, have not been able yet to mimic long-distance water transport under negative pressure, except on a very small scale and under very controlled and unrealistic conditions (Wheeler & Stroock 2008; Boatwright et al. 2015; Shi et al. 2019). Because we do not fully understand why xylem sap does not embolise continuously under negative pressure, sap flow in plants represents one of the longest standing questions in plant biology. The three-dimensional structure of pit membranes, combined with the dynamic surface tension of amphiphilic lipids associated with pit membranes, provide a promising new approach to investigate mechanisms of air-seeding and could contribute to the development of man-made evaporation driven transport devices. It is very clear that pit membranes are required for water transport under negative pressure, because such transport was found to be almost impossible in stem segments of *Fagus sylvatica* (Fagaceae) and *Populus tremula* (Salicaceae) after artificial removal of pit membranes by cellulase treatment (Dusotoit-Coucaud et al. 2014). Similar observations of completely open vessels that very easily embolise under negative pressure when constructing centrifuge-based vulnerability curves (Torres-Ruiz et al. 2017; Du et al. 2019) also suggest that nanoporous media are crucial components of systems designed for efficient and reliable water transport under negative pressure.

1 Finally, mechanical properties of pit membranes deserve more attention, especially with respect  
2 to fresh, fully hydrated pit membranes that have never experienced any shrinkage due to  
3 aspiration or dehydration. Atomic force microscopy and nano-indentation represent important  
4 approaches and should be complemented with modelling. We also require a better understanding  
5 of potential deformation processes of pit membranes at the nanoscale, when pit membrane  
6 shrinkage happens in plants, and whether this process is associated with a loss of their hydraulic  
7 function. The molecular strain in pit membranes could also be quantified by studying band shifts  
8 based on near infrared spectroscopy. From the various forms of spectroscopy that have been  
9 successfully applied to monitor molecular strain in cellulose under load (Hinterstoisser et al.  
10 2003; Štuncová et al. 2006; Altaner et al. 2014; Guo & Altaner 2018), Raman microscopy  
11 (Gierlinger et al. 2006) could provide a high resolution to study pit membranes.

## 13 **Acknowledgements**

14 Financial support is acknowledged to LK, CC, and SJ by a research grant from the German  
15 Research Foundation (JA 2174/5-1; nr. 383393940), by the Baden-Württemberg Ministerium für  
16 Wissenschaft, Forschung und Kunst (project 7533-7-11.10-16), and to H.J.S. and SJ by the  
17 National Science Foundation (IOS-1754850). We acknowledge the Paul Scherrer Institut,  
18 Villigen, Switzerland for provision of synchrotron radiation beamtime at the cSAXS beamline of  
19 the SLS (projects 20171559 and 20180784). We also thank Andrea Huppenberger, Scott  
20 McAdam, Luciano Pereira, Melvin Tyree, and Paul Walther for fruitful discussions, suggestions,  
21 and practical assistance in the lab.

## 1   **References**

- 2   Altaner CM, Thomas LH, Fernandes AN, Jarvis MC. 2014. How Cellulose Stretches: Synergism  
3   between Covalent and Hydrogen Bonding. *Biomacromolecules* 15: 791--798.  
4   DOI: 10.1021/bm401616n
- 5   Askenasy E. 1895. Über das Saftsteigen. In: *Sitzungsber Heidelberg Akad Wiss. Heidelberg:*  
6   Carl Winter; p. 23.
- 7   Bamber RK. 1961. Staining reaction of the pit membrane of wood cells. *Nature* 191-: 409.  
8   DOI: 10.1038/191409b0
- 9   Barnett JR. 1981. Xylem Cell Development. In: *Secondary xylem cell development*. Castle  
10   House Publications Ltd, Tunbridge Wells.
- 11   Barnett JR. 1982. Plasmodesmata and pit development in secondary xylem elements. *Planta* 155:  
12   251--260. DOI: 10.1007/BF00392724
- 13   Barnett JR, Harris JM. 1975. Early stages of bordered pit formation in radiata pine. *Wood Sci.*  
14   *Technol.* 9: 233--241. DOI: 10.1007/BF00364640
- 15   Bartlett MK, Klein T, Jansen S, Choat B, Sack L. 2016. The correlations and sequence of plant  
16   stomatal, hydraulic, and wilting responses to drought. *PNAS* 113: 13098--13103.
- 17   Benayoun J, Catesson AM, Czaninski Y. 1981. A cytochemical study of differentiation and  
18   breakdown of vessel end walls. *Ann. Bot.* 47: 687--698.
- 19   Bliss MC. 1921. The Vessel in Seed Plants. *Bot. Gaz.* 71: 314--326. DOI: 10.1086/332838

- 1 Boatwright A, Hughes S, Barry J. 2015. The height limit of a siphon. *Sci. Rep.* 5, 16790.  
2 DOI: 10.1038/srep16790
- 3 Bouche PS, Larter M, Domec J-C, Burlett R, Gasson P, Jansen S, Delzon S. 2014. A broad  
4 survey of hydraulic and mechanical safety in the xylem of conifers. *J. Exp. Bot.* 65: 4419--4431.  
5 DOI: 10.1093/jxb/eru218
- 6 Bourdon M, Kalmbach L, Helariutta Y. 2017. Plant casculature: selective membrane-to-  
7 microtubule tethering patterns the xylem cell wall. *Curr. Biol.* 27: R842--R844.  
8 DOI: 10.1016/j.cub.2017.07.044
- 9 Brodersen CR, McElrone AJ, Choat B, Lee EF, Shackel KA, Matthews MA. 2013. In vivo  
10 visualizations of drought-induced embolism spread in *Vitis vinifera*. *Plant Physiol.* 161: 1820--  
11 1829. DOI: 10.1104/pp.112.212712
- 12 Brodribb TJ, Bienaimé D, Marmottant P. 2016. Revealing catastrophic failure of leaf networks  
13 under stress. *PNAS* 113: 4865--4869. DOI: 10.1073/pnas.1522569113
- 14 Buesch C, Smith SW, Eschbach P, Conley JF, Simonsen J. 2016. The microstructure of cellulose  
15 nanocrystal aerogels as revealed by transmission electron microscope tomography.  
16 *Biomacromolecules* 17: 2956--2962. DOI: 10.1021/acs.biomac.6b00764
- 17 Buono RA, Hudecek R, Nowack MK. 2019. Plant proteases during developmental programmed  
18 cell death. *J. Exp. Bot.* 70: 2097--2112. DOI: 10.1093/jxb/erz072
- 19 Butterfield BG. 1995. Vessel element differentiation. In: *The Cambial Derivatives*. Gebrüder  
20 Borntraeger, Berlin, Stuttgart.

- 1 Capron M, Tordjeman Ph, Charru F, Badel E, Cochard H. 2014. Gas flow in plant microfluidic  
2 networks controlled by capillary valves. *Phys. Rev. E.* 89, 033019.  
3 DOI: 10.1103/PhysRevE.89.033019
- 4 Carlquist S, Schneider EL. 2001. Vessels in ferns: structural, ecological, and evolutionary  
5 significance. *Am. J. Bot.* 88: 1--13. DOI: 10.2307/2657121
- 6 Chaffey N, Barlow P, Barnett J. 2000. A cytoskeletal basis for wood formation in angiosperm  
7 trees: the involvement of microfilaments. *Planta* 210: 890--896. DOI: 10.1007/s004250050694
- 8 Chaffey N, Barnett JR, Barlow PW. 1997. Cortical microtubule involvement in bordered pit  
9 formation in secondary xylem vessel elements of *Aesculus hippocastanum* L.  
10 (*Hippocastanaceae*): A correlative study using electron microscopy and indirect  
11 immunofluorescence microscopy. *Protoplasma* 197: 64--75. DOI: 10.1007/BF01279885
- 12 Chaffey N, Barnett JR, Barlow PW. 1999. A cytoskeletal basis for wood formation in  
13 angiosperm trees: the involvement of cortical microtubules. *Planta* 208: 19--30.  
14 DOI: 10.1007/s004250050530
- 15 Chaffey N, Cholewa E, Regan S, Sundberg B. 2002. Secondary xylem development in  
16 *Arabidopsis*: a model for wood formation. *Physiol. Plant.* 114: 594--600. DOI: 10.1034/j.1399-  
17 3054.2002.1140413.x
- 18 Choat B, Badel E, Burlett R, Delzon S, Cochard H, Jansen S. 2016. Noninvasive measurement of  
19 vulnerability to drought-induced embolism by x-ray microtomography. *Plant Physiol.* 170:273--  
20 282. DOI: 10.1104/pp.15.00732

- 1 Choat B, Ball M, Luly J, Holtum J. 2003. Pit membrane porosity and water stress-induced  
2 cavitation in four co-existing dry rainforest tree species. *Plant Physiol.* 131:41--48.  
3 DOI: 10.1104/pp.014100
- 4 Choat B, Brodie TW, Cobb AR, Zwieniecki MA, Holbrook NM. 2006. Direct measurements of  
5 intervessel pit membrane hydraulic resistance in two angiosperm tree species. *Am. J. Bot.*  
6 93:993--1000. 1000. DOI: 10.3732/ajb.93.7.993
- 7 Choat B, Cobb AR, Jansen S. 2008. Structure and function of bordered pits: new discoveries and  
8 impacts on whole-plant hydraulic function. *New Phytol.* 177:608--626. DOI: 10.1111/j.1469-  
9 8137.2007.02317.x
- 10 Choat B, Jansen S, Brodribb TJ, Cochard H, Delzon S, Bhaskar R, Bucci SJ, Feild TS, Gleason  
11 SM, Hacke UG, et al. 2012. Global convergence in the vulnerability of forests to drought. *Nature*  
12 491: 752--755. DOI: 10.1038/nature11688
- 13 Choat B, Jansen S, Zwieniecki MA, Smets E, Holbrook NM. 2004. Changes in pit membrane  
14 porosity due to deflection and stretching: the role of vested pits. *J. Exp. Bot.* 55: 1569--1575.  
15 DOI: 10.1093/jxb/erh173
- 16 Christensen-Dalsgaard KK, Tyree MT, Mussone PG, Meinzer F. 2011. Surface tension  
17 phenomena in the xylem sap of three diffuse porous temperate tree species. *Tree Physiol.* 31:  
18 361--368. DOI: 10.1093/treephys/tpr018
- 19 Christman MA, Sperry JS. 2010. Single-vessel flow measurements indicate scalariform  
20 perforation plates confer higher flow resistance than previously estimated. *Plant Cell Environ.*  
21 33: 431--443. DOI: 10.1111/j.1365-3040.2009.02094.x

- 1 Dixon HH. 1914. Transpiration and the ascent of sap in plants. Macmillan and Co., London.
- 2 Dixon HH, Joly J. 1895. On the ascent of sap. Philos. Trans. Royal Soc. Lond. (B) 186: 563--  
3 576. DOI: 10.1098/rstb.1895.0012
- 4 Donaldson LA, Cairns M, Hill SJ. 2018. Comparison of micropore distribution in cell walls of  
5 softwood and hardwood xylem. Plant Physiol. 178: 1142--1153. DOI: 10.1104/pp.18.00883
- 6 Donaldson LA, Kroese HW, Hill SJ, Franich RA. 2015. Detection of wood cell wall porosity  
7 using small carbohydrate molecules and confocal fluorescence microscopy. J. Microsc. 259: 228-  
8 -236. DOI: 10.1111/jmi.12257
- 9 van Doorn WG, Hiemstra T, Fanourakis D. 2011. Hydrogel regulation of xylem water flow: An  
10 alternative hypothesis. Plant Physiol. 157: 1642--1649. DOI: 10.1104/pp.111.185314
- 11 Dória L, Podadera D, Lima R, Lens F, Marcati C. 2019. Axial sampling height outperforms site  
12 as predictor of wood trait variation. IAWA J. 24: 1--S3. DOI: 10.1163/22941932-40190245
- 13 Du G, Feng F, Wang Y, Tyree MT. 2019. Do nano-particles cause recalcitrant vulnerability  
14 curves in Robinia? Testing with a four-cuvette Cochard rotor and with water extraction curves.  
15 Tree Physiol. 39: 156--165. DOI: 10.1093/treephys/tpy051
- 16 Dusotoit-Coucaud A, Brunel N, Tixier A, Cochard H, Herbette S. 2014. Hydrolase treatments  
17 help unravel the function of intervessel pits in xylem hydraulics. Physiol. Plant. 150: 388--396.  
18 DOI: 10.1111/ppl.12092

- 1 Dute R, Daniel Jandrlich M, Thornton S, Callahan N, Hansen C. 2011. Tori in species of  
2 *Diarthron*, *Stellera* and *Thymelaea* (*Thymelaeaceae*). IAWA J. 32: 54--66.  
3 DOI: 10.1163/22941932-90000042
- 4 Dute R, Patel J, Jansen S. 2010. Torus-bearing pit membranes in *Cercocarpus*. IAWA J. 31:53--  
5 66. DOI: 10.1163/22941932-90000005
- 6 Ellerby DJ, Ennos AR. 1998. Resistances to fluid flow of model xylem vessels with simple and  
7 scalariform perforation plates. J. Exp. Bot. 49: 979--985. DOI: 10.1093/jxb/49.323.979
- 8 Escamez S, Stael S, Vainonen JP, Willems P, Jin H, Kimura S, Van Breusegem F, Gevaert K,  
9 Wrzaczek M, Tuominen H. 2019. Extracellular peptide Kratos restricts cell death during vascular  
10 development and stress in Arabidopsis. J. Exp. Bot. 70: 2199--2210. DOI: 10.1093/jxb/erz021
- 11 Ewart AJ. 1906. The ascent of water in trees. Philos. Trans. Royal Soc. Lond. (B) 198: 41-- 85.
- 12 Fardim P, Moreno T, Holmbom B. 2005. Anionic groups on cellulosic fiber surfaces investigated  
13 by XPS, FTIR-ATR, and different sorption methods. J. Colloid Interface Sci. 290: 383--391.  
14 DOI: 10.1016/j.jcis.2005.04.067
- 15 Funada R. 2000. Control of wood structure. In: P Nick (ed). Plant Microtubules: Potential for  
16 Biotechnology. Springer Verlag, Berlin, Heidelberg.
- 17 Gierlinger N, Schwanninger M, Reinecke A, Burgert I. 2006. Molecular changes during tensile  
18 deformation of single wood fibers followed by Raman microscopy. Biomacromolecules 7: 2077-  
19 2081. DOI: 10.1021/bm060236g
- 20 Gor GY, Huber P, Bernstein N. 2017. Adsorption-induced deformation of nanoporous  
21 materials—A review. Appl. Phys. Rev. 4, 011303. DOI: 10.1063/1.4975001



- 1 Guo F, Altaner CM. 2018. Molecular deformation of wood and cellulose studied by near infrared  
2 spectroscopy. Carbohydr. Polym. 197: 1--8. DOI: 10.1016/j.carbpol.2018.05.064
- 3 Hacke U, Stiller V, Sperry J, Pittermann J, McCulloh KA. 2001. Cavitation fatigue. Embolism  
4 and refilling cycles can weaken the cavitation resistance of xylem. Plant Physiol. 125: 779--86.  
5 DOI: 10.1104/pp.125.2.779
- 6 Hacke UG, Sperry JS, Wheeler JK, Castro L. 2006. Scaling of angiosperm xylem structure with  
7 safety and efficiency. Tree Physiol. 26: 689--701. DOI: 10.1093/treephys/26.6.689
- 8 Herbette S, Bouchet B, Brunel N, Bonnin E, Cochard H, Guillon F. 2015. Immunolabelling of  
9 intervessel pits for polysaccharides and lignin helps in understanding their hydraulic properties in  
10 *Populus tremula* × *alba*. Ann. Bot. 115: 187--199. DOI: 10.1093/aob/mcu232
- 11 Hillabrand RM, Hacke UG, Lieffers VJ. 2016. Drought-induced xylem pit membrane damage in  
12 aspen and balsam poplar. Plant Cell Environ. 39: 2210--2220. DOI: 10.1111/pce.12782
- 13 Hinterstoisser B, Akerholm M, Salmén L. 2003. Load distribution in native cellulose.  
14 Biomacromolecules 4: 1232--1237. DOI: 10.1021/bm030017k
- 15 Holler M, Raabe J, Diaz A, Guizar-Sicairos M, Wepf R, Odstřil M, Shaik FR, Panneels V,  
16 Menzel A, Sarafimov B, et al. 2018. OMNY-A tOMography Nano crYo stage. Rev. Sci. Instrum.  
17 89: 043706. DOI: 10.1063/1.5020247
- 18 Iakimova ET, Woltering EJ. 2017. Xylogenesis in zinnia (*Zinnia elegans*) cell cultures:  
19 unravelling the regulatory steps in a complex developmental programmed cell death event.  
20 Planta 245: 681--705. DOI: 10.1007/s00425-017-2656-1

- 1 Ito J, Fukuda H. 2002. ZEN1 is a key enzyme in the degradation of nuclear DNA during  
2 programmed cell death of tracheary elements. *Plant Cell* 14: 3201--3211.  
3 DOI: 10.1105/tpc.006411
- 4 Jansen S, Choat B, Pletsers A. 2009. Morphological variation of intervessel pit membranes and  
5 implications to xylem function in angiosperms. *Am. J. Bot.* 96: 409--419.  
6 DOI: 10.3732/ajb.0800248
- 7 Jansen S, Dute R, Allison J, Rabaey D. 2010. Torus-bearing pit membranes in species of  
8 *Osmanthus*. *IAWA J.* 31: 217--226. DOI: 10.1163/22941932-90000018
- 9 Jansen S, Klepsch M, Li S, Kotowska M, Schiele S, Zhang Y, Schenk H. 2018. Challenges in  
10 understanding air-seeding in angiosperm xylem. *Acta Hort.* 1222: 13--20.  
11 DOI: 10.17660/ActaHortic.2018.1222.3
- 12 Jansen S, McAdam S. 2019. Pits with aspiration explain life expectancy of a conifer species.  
13 *PNAS* 116: 14794--14796. DOI: 10.1073/pnas.1909866116
- 14 Jansen S, Pletsers A, Sano Y. 2008. The effect of preparation techniques on SEM-imaging of pit  
15 membranes. *IAWA J.* 29: 161--178. DOI: 10.1163/22941932-90000177
- 16 Jansen S, Sano Y, Choat B, Rabaey D, Lens F, Dute RR. 2007. Pit membranes in tracheary  
17 elements of *Rosaceae* and related families: new records of tori and pseudotori. *Am. J. Bot.* 94:  
18 503--514. DOI: 10.3732/ajb.94.4.503
- 19 Jansen S, Schuldt B, Choat B. 2015. Current controversies and challenges in applying plant  
20 hydraulic techniques. *New Phytol.* 205: 961--964. DOI: 10.1111/nph.13229

- 1 Johnson D, Eckart P, Alsamadisi N, Noble H, Martin C, Spicer R. 2018. Polar auxin transport is  
2 implicated in vessel differentiation and spatial patterning during secondary growth in *Populus*.  
3 Am. J. Bot. 105: 186--196. DOI: 10.1002/ajb2.1035
- 4 Juniper BE. 1977. Some speculations on the possible roles of the plasmodesmata in the control  
5 of differentiation. J. Theoret. Biol. 66: 583--592. DOI: 10.1016/0022-5193(77)90304-6
- 6 Kaushik M, Fraschini C, Chauve G, Putaux J-L and Moores A. 2015. Transmission electron  
7 microscopy for the characterization of cellulose nanocrystals. In: K Maaz (ed.), The  
8 Transmission Electron Microscope - Theory and Applications: pp 12--163. IntechOpen, London.  
9 DOI: 10.5772/60985
- 10 Kenrick P, Crane PR. 1991. Water-conducting cells in early fossil land plants: Implications for  
11 the early evolution of tracheophytes. Bot. Gaz. 152: 335--356. DOI: 10.1086/337897
- 12 Kenrick P, Crane PR. 1997. The origin and early evolution of plants on land. Nature 389: 33--39.  
13 DOI: 10.1038/37918
- 14 Kerr T, Bailey IW. 1934. The cambium and its derivative tissues: X. Structure, optical properties  
15 and chemical composition of the so-called middle lamella. J. Arnold Arbor. 15: 327--349.
- 16 Kim JS, Daniel G. 2013. Developmental localization of homogalacturonan and xyloglucan  
17 epitopes in pit membranes varies in two poplar species. IAWA J. 34: 245--262.  
18 DOI: 10.1163/22941932-00000021

- 1 Kim JS, Sandquist D, Sundberg B, Daniel G. 2012. Spatial and temporal variability of xylan  
2 distribution in differentiating secondary xylem of hybrid aspen. *Planta* 235: 1315--1330.  
3 DOI: 10.1007/s00425-011-1576-8
- 4 Kininmonth JA. 1971. Permeability and fine structure of certain hardwoods and effects on  
5 drying. I. Transverse permeability of wood to micro-filtered water. *Holzforschung* 25: 127--133.  
6 DOI: 10.1515/hfsg.1971.25.4.127
- 7 Kininmonth JA. 1972. Permeability and fine structure of certain hardwoods and effects on  
8 drying. II. Differences in fine structure of *Nothofagus fusca* sapwood and heartwood.  
9 *Holzforschung* 26: 32--38. DOI: 10.1515/hfsg.1972.26.1.32
- 10 Kitin P, Funada R. 2016. Earlywood vessels in ring-porous trees become functional for water  
11 transport after bud burst and before the maturation of the current-year leaves. *IAWA J.* 37: 315--  
12 331. DOI: 10.1163/22941932-20160136
- 13 Klepsch MM, Schmitt M, Paul Knox J, Jansen S. 2016. The chemical identity of intervessel pit  
14 membranes in *Acer* challenges hydrogel control of xylem hydraulic conductivity. *AoB Plants* 8:  
15 plw052. DOI: 10.1093/aobpla/plw052
- 16 Klepsch MM, Zhang Y, Kotowska MM, Lamarque LJ, Nolf M, Schuldt B, Torres-Ruiz JM, Qin  
17 D-W, Choat B, Delzon S, et al. 2018. Is xylem of angiosperm leaves less resistant to embolism  
18 than branches? Insights from microCT, hydraulics, and anatomy. *J. Exp. Bot.* 69: 5611--5623.
- 19 Kotowska MM, Thom R, Zhang Y, Schenk HJ, Jansen S. 2019. Within-tree variability and  
20 sample storage effects of bordered pit membranes in xylem of *Acer pseudoplatanus*. *Trees*.  
21 DOI: 10.1007/s00468-019-01897-4.

- 1 Kroon-Batenburg LMJ, Kroon JW, Northolt MG. 1986. Chain modulus and intramolecular  
2 hydrogen bonding in native and regenerated cellulose fibers. *Polym. Commun.* 27: 290--292.
- 3 Lee J, Holbrook NM, Zwieniecki MA. 2012. Ion induced changes in the structure of bordered pit  
4 membranes. *Front. Plant Sci.* 3: 55. DOI: 10.3389/fpls.2012.00055.
- 5 Lens F, Sperry JS, Christman MA, Choat B, Rabaey D, Jansen S. 2011. Testing hypotheses that  
6 link wood anatomy to cavitation resistance and hydraulic conductivity in the genus *Acer*. *New*  
7 *Phytol.* 190: 709--723. DOI: 10.1111/j.1469-8137.2010.03518.x
- 8 Li S, Lens F, Espino S, Karimi Z, Klepsch M, Schenk HJ, Schmitt M, Schuldt B, Jansen S. 2016.  
9 Intervessel pit membrane thickness as a key determinant of embolism resistance in angiosperm  
10 xylem. *IAWA J.* 37: 152--171. DOI: 10.1163/22941932-20160128
- 11 Liese W. 2007. Electron microscopy of wood : the pioneering year. *Mitt Bundesforschungsanst*  
12 *Forst-Holzwirtschaft Hamburg* 223: 3--12.
- 13 Liese W, Côté WA. 1960. Electron microscopy of wood: results of the first ten years of research.  
14 *Proceedings of the Fifth World Forestry Congress, Seattle*, 2: 1288--1298.
- 15 Lindström T, Wågberg L, Larsson T. 2005. On the nature of joint strength in paper - A review of  
16 dry and wet strength resins in paper manufacturing. *Nord Pulp Paper Res. J.* 31: 459--468.  
17 DOI: 10.3183/npprj-2016-31-03-p459-468
- 18 Martínez-Sanz M, Pettolino F, Flanagan B, Gidley MJ, Gilbert EP. 2017. Structure of cellulose  
19 microfibrils in mature cotton fibres. *Carbohydr. Polym.* 175: 450--463.  
20 DOI: 10.1016/j.carbpol.2017.07.090

- 1    Meylan BA, Butterfield BG. 1981. Perforation plant differentiation in the vessels of hardwoods.  
2    In: JR Barnett (ed.), Xylem Cell Development. Castle House Publications Ltd., Tunbridge  
3    Wells.
- 4    Meyra AG, Kuz VA, Zarragoicoechea GJ. 2007. Geometrical and physicochemical  
5    considerations of the pit membrane in relation to air seeding: the pit membrane as a capillary  
6    valve. *Tree Physiol.* 27: 1401--1405. DOI: 10.1093/treephys/27.10.1401
- 7    Muhammad AF, Sattler R. 1982. Vessel structure of *Gnetum* and the origin of angiosperms. *Am.*  
8    *J. Bot.* 69: 1004--1021. DOI: 10.1002/j.1537-2197.1982.tb13345.x
- 9    Murmanis L, Chudnoff M. 1979. Lateral flow in beech and birch as revealed by the electron  
10    microscope. *Wood Sci. Technol.* 13: 79--87. DOI: 10.1007/BF00368601
- 11    Nardini A, Salleo S, Jansen S. 2011. More than just a vulnerable pipeline: xylem physiology in  
12    the light of ion-mediated regulation of plant water transport. *J. Exp. Bot.* 62: 4701--4718.  
13    DOI: 10.1093/jxb/err208
- 14    Neumann M, Hirsch C, Staněk J, Beneš V, Schmidt V. 2019. Estimation of geodesic tortuosity  
15    and constrictivity in stationary random closed sets. *Scand. J. Stat.* 46: 848--884.  
16    DOI: 10.1111/sjos.12375
- 17    Neumann PM, Weissman R, Stefano G, Mancuso S. 2010. Accumulation of xylem transported  
18    protein at pit membranes and associated reductions in hydraulic conductance. *J. Exp. Bot.* 61:  
19    1711--1717. DOI: 10.1093/jxb/erq037

- 1 O'Brien TP. 1970. Further observations on hydrolysis of the cell wall in the xylem. *Protoplasma*  
2 69: 1--14. DOI: 10.1007/BF01276648
- 3 O'Brien TP. 1981. The primary xylem. In: JR Barnett (ed.), *Xylem Cell Development*. Castle  
4 House Publications Ltd., Tunbridge Wells.
- 5 Oda Y, Fukuda H. 2013. Rho of plant GTPase signaling regulates the behavior of *Arabidopsis*  
6 Kinesin-13A to establish secondary cell wall patterns. *Plant Cell* 25: 4439--4450.  
7 DOI: 10.1105/tpc.113.117853
- 8 Odstreil M, Holler M, Raabe J, Sepe A, Sheng X, Vignolini S, Schroer CG, Guizar-Sicairos M.  
9 2019. Ab initio nonrigid X-ray nanotomography. *Nat. Commun.* 10, 2600.  
10 DOI: 10.1038/s41467-019-10670-7
- 11 Osorio DA, Seifried B, Moquin P, Grandfield K, Cranston ED. 2018. Morphology of cross-  
12 linked cellulose nanocrystal aerogels: cryo-templating versus pressurized gas expansion  
13 processing. *J. Mater. Sci.* 53: 9842--9860. DOI: 10.1007/s10853-018-2235-2
- 14 Pan R, Tyree MT. 2019. How does water flow from vessel to vessel? Further investigation of the  
15 tracheid bridge concept. *Tree Physiol.* 39: 1019--1031. DOI: 10.1093/treephys/tpz015
- 16 Park JY, Go T, Ryu J, Lee SJ. 2019. Air spreading through wetted cellulose membranes:  
17 implications for the safety function of hydraulic valves in plants. *Phys. Rev. E* 100, 032409.  
18 DOI: 10.1103/PhysRevE.100.032409
- 19 Pereira L, Flores-Borges DNA, Bittencourt PRL, Mayer JLS, Kiyota E, Araújo P, Jansen S,  
20 Freitas RO, Oliveira RS, Mazzafera P. 2018. Infrared nanospectroscopy reveals the chemical

- 1 nature of pit membranes in water-conducting cells of the plant xylem. *Plant Physiol.* 177: 1629--  
2 1638. DOI: 10.1104/pp.18.00138
- 3 Pesacreta TC, Groom LH, Rials TG. 2005. Atomic force microscopy of the intervessel pit  
4 membrane in the stem of *Sapium sebiferum* (*Euphorbiaceae*). *IAWA J.* 26: 397--426.  
5 DOI: 10.1163/22941932-90000124
- 6 Petty JA, Preston RD. 1972. The aspiration of bordered pits in conifer wood. *Proc. Royal Soc.*  
7 *Lond. (B)* 181: 395--406. DOI: 10.1098/rspb.1972.0057
- 8 Peyrega C, Jeulin D. 2013. Estimation of tortuosity and reconstruction of geodesic paths in 3D.  
9 *Image Anal. Stereol.* 32: 27--43.
- 10 Pfautsch S, Aspinwall MJ, Drake JE, Chacon-Doria L, Langelaan RJA, Tissue DT, Tjoelker MG,  
11 Lens F. 2018. Traits and trade-offs in whole-tree hydraulic architecture along the vertical axis of  
12 *Eucalyptus grandis*. *Ann. Bot.* 121: 129--141.
- 13 Pittermann J, Limm E, Rico C, Christman MA. 2011. Structure-function constraints of tracheid-  
14 based xylem: a comparison of conifers and ferns. *New Phytol.* 192: 449--461.  
15 DOI: 10.1111/j.1469-8137.2011.03817.x
- 16 Pittermann J, Sperry JS, Hacke UG, Wheeler JK, Sikkema EH. 2005. Torus-margo pits help  
17 conifers compete with angiosperms. *Science* 310: 1924--1924. DOI: 10.1126/science.1120479
- 18 Plavcová L, Hacke UG. 2011. Heterogeneous distribution of pectin epitopes and calcium in  
19 different pit types of four angiosperm species. *New Phytol.* 192: 885--897. DOI: 10.1111/j.1469-  
20 8137.2011.03842.x



- 1 Plavcová L, Jansen S, Klepsch M, Hacke UG. 2013. Nobody's perfect: can irregularities in pit  
2 structure influence vulnerability to cavitation? *Front. Plant Sci.* 4: 453.  
3 DOI: 10.3389/fpls.2013.00453
- 4 Rabaey D, Lens F, Huysmans S, Smets E, Jansen S. 2008. A comparative ultrastructural study of  
5 pit membranes with plasmodesmata associated thickenings in four angiosperm species.  
6 *Protoplasma* 233: 255--262. DOI: 10.1007/s00709-008-0019-2
- 7 Reza M, Kontturi E, Jääskeläinen A-S, Vuorinen T, Ruokolainen J. 2015. Transmission electron  
8 microscopy for wood and fiber analysis – A review. *BioResources* 10: 6230-6261--6261.  
9 DOI: 10.15376/biores.10.3.
- 10 Riemersma JC. 1968. Osmium tetroxide fixation of lipids for electron microscopy. A possible  
11 reaction mechanism. *Biochim. Biophys. Acta* 152: 718--727. DOI: 10.1016/0005-  
12 2760(68)90118-5
- 13 Robards AW, Humpherson PG. 1967. Microtubules and angiosperm bordered pit formation.  
14 *Planta* 77: 233--238. DOI: 10.1007/BF00385293
- 15 Rongpipi S, Ye D, Gomez ED, Gomez EW. 2018. Progress and opportunities in the  
16 characterization of cellulose - An important regulator of cell wall growth and mechanics. *Front.*  
17 *Plant Sci.* 9: 1894. DOI: 10.3389/fpls.2018.01894
- 18 Roth-Nebelsick A. 2019. It's contagious: calculation and analysis of xylem vulnerability to  
19 embolism by a mechanistic approach based on epidemic modeling. *Trees* 33: 1519-1533  
20 DOI: 10.1007/s00468-019-01891-w

- 1 Rudman P. 1966. Studies in wood preservation Pt. II. Movement of aqueous solutions through  
2 the pits and cell walls of eucalypt sapwoods. *Holzforschung* 20: 57--60.  
3 DOI: 10.1515/hfsg.1966.20.2.57
- 4 Ruel K, Nishiyama Y, Joseleau J-P. 2012. Crystalline and amorphous cellulose in the secondary  
5 walls of *Arabidopsis*. *Plant Sci.* 193--194: 48--61. DOI: 10.1016/j.plantsci.2012.05.008
- 6 Sano Y. 2005. Inter- and intraspecific structural variations among intervacular pit membranes,  
7 as revealed by field-emission scanning electron microscopy. *Am. J. Bot.* 92: 1077--1084.  
8 92:1077--1084. DOI: 10.3732/ajb.92.7.1077
- 9 Sano Y, Morris H, Shimada H, Ronse De Craene LP, Jansen S. 2011. Anatomical features  
10 associated with water transport in imperforate tracheary elements of vessel-bearing angiosperms.  
11 *Ann. Bot.* 107: 953--964. DOI: 10.1093/aob/mcr042
- 12 Sano Y, Utsumi Y, Nakada R. 2013. Homoplastic occurrence of perforated pit membranes and  
13 torus-bearing pit membranes in ancestral angiosperms as observed by field-emission scanning  
14 electron microscopy. *J. Wood Sci.* 59: 95--103. DOI: 10.1007/s10086-012-1304-4
- 15 Santiago M, Pagay V, Stroock AD. 2013. Impact of Electroviscosity on the Hydraulic  
16 Conductance of the Bordered Pit Membrane: A Theoretical Investigation. *Plant Physiol.* 163:  
17 999--1011. DOI: 10.1104/pp.113.219774
- 18 Schacht H. 1859. Über die Tüpfel der Gefäss- und Holzzellen. *Botanische Zeitung* 17: 238--239.
- 19 Schenk HJ, Espino S, Rich-Cavazos SM, Jansen S. 2018. From the sap's perspective: The nature  
20 of vessel surfaces in angiosperm xylem. *Am. J. Bot.* 105: 172--185. DOI: 10.1002/ajb2.1034

- 1 Schenk HJ, Espino S, Romo DM, Nima N, Do AYT, Michaud JM, Papahadjopoulos-Sternberg
- 2 B, Yang J, Zuo YY, Steppe K, Jansen S. 2017. Xylem surfactants introduce a new element to the
- 3 Cohesion-Tension theory. *Plant Physiol.* 173: 1177--1196. DOI: 10.1104/pp.16.01039
- 4 Schenk HJ, Michaud JM, Espino S, Melendres T, Roth MR, Welti R, Kaack L, and Jansen S.
- 5 2019. Lipids in xylem sap of woody plants across the angiosperm phylogeny. *bioRxiv*:763771.
- 6 <https://www.biorxiv.org/content/10.1101/763771v1>
- 7 Schenk HJ, Steppe K, Jansen S. 2015. Nanobubbles: a new paradigm for air-seeding in xylem.
- 8 *Trends Plant Sci.* 20: 199--205. DOI: 10.1016/j.tplants.2015.01.008
- 9 Schmid R, Machado RD. 1968. Pit membranes in hardwoods—Fine structure and development.
- 10 *Protoplasma* 66: 185--204. DOI: 10.1007/BF01252532
- 11 Schmitz N, Jansen S, Verheyden A, Kairo JG, Beeckman H, Koedam N. 2007. Comparative
- 12 anatomy of intervessel pits in two mangrove species growing along a natural salinity gradient in
- 13 Gazi Bay, Kenya. *Ann. Bot.* 100: 271--281. DOI: 10.1093/aob/mcm103
- 14 Scholz A, Rabaey D, Stein A, Cochard H, Smets E, Jansen S. 2013. The evolution and function
- 15 of vessel and pit characters with respect to cavitation resistance across 10 *Prunus* species. *Tree*
- 16 *Physiol.* 33: 684--694. DOI: 10.1093/treephys/tpt050
- 17 Schulte PJ, Gibson AC. 1988. Hydraulic conductance and tracheid anatomy in six species of
- 18 extant seed plants. *Can. J. Bot.* 66: 1073--1079. DOI: 10.1139/b88-153
- 19 Shahmoradian SH, Tsai EHR, Diaz A, Guizar-Sicairos M, Raabe J, Spycher L, Britschgi M, Ruf
- 20 A, Stahlberg H, Holler M. 2017. Three-Dimensional Imaging of Biological Tissue by Cryo X-
- 21 Ray Ptychography. *Sci. Rep.* 7: 6291. DOI: 10.1038/s41598-017-05587-4

- 1 Shane MW, McCully ME, Canny MJ. 2000. Architecture of branch-root junctions in maize:  
2 structure of the connecting xylem and the porosity of pit membranes. *Ann. Bot.* 85: 613--624.  
3 DOI: 10.1006/anbo.2000.1113
- 4 Shi W, Vieitez JR, Berrier AS, Roseveare MW, Surinach DA, Srijanto BR, Collier CP, Boreyko  
5 JB. 2019. Self-stabilizing transpiration in synthetic leaves. *ACS Appl. Mater. Interfaces* 11:  
6 13768--13776. DOI: 10.1021/acsami.9b00041
- 7 Shou D, Fan J, Ding F. 2011. Hydraulic permeability of fibrous porous media. *Int. J. Heat Mass*  
8 *Transf.* 54: 4009--4018. DOI: 10.1016/j.ijheatmasstransfer.2011.04.022
- 9 Skelton RP, Brodribb TJ, Choat B. 2017. Casting light on xylem vulnerability in an herbaceous  
10 species reveals a lack of segmentation. *New Phytol.* 214: 561--569.
- 11 Smetana O, Mäkilä R, Lyu M, Amiryousefi A, Rodríguez FS, Wu M-F, Solé-Gil A, Gavarrón  
12 ML, Siligato R, Miyashima S, et al. 2019. High levels of auxin signaling define the stem-cell  
13 organizer of the vascular cambium. *Nature* 565: 485--489. DOI: 10.1038/s41586-018-0837-0
- 14 Sperry J, Tyree M. 1988. Mechanism of water stress-induced xylem embolism. *Plant Physiol.* 88:  
15 581--7. DOI: 10.1104/pp.88.3.581
- 16 Sperry JS, Hacke UG. 2004. Analysis of circular bordered pit function I. Angiosperm vessels  
17 with homogenous pit membranes. *Am. J. Bot.* 91: 369--385. DOI: 10.3732/ajb.91.3.369
- 18 Sperry JS, Hacke UG, Wheeler JK. 2005. Comparative analysis of end wall resistivity in xylem  
19 conduits. *Plant Cell Environ.* 28: 456--465. DOI: 10.1111/j.1365-3040.2005.01287.x

- 1 Stiller V, & Sperry JS. (2002) Cavitation fatigue and its reversal in sunflower (*Helianthus*  
2 *annuus* L.). J. Exp. Bot. 53: 1155--1161. DOI: 10.1093/jexbot/53.371.1155
- 3 Šturcová A, Eichhorn SJ, Jarvis MC. 2006. Vibrational spectroscopy of biopolymers under  
4 mechanical stress: Processing cellulose spectra using bandshift difference integrals.  
5 Biomacromolecules 7: 2688--2691. DOI: 10.1021/bm060457m
- 6 Sugiyama Y, Nagashima Y, Wakazaki M, Sato M, Toyooka K, Fukuda H, Oda Y. 2019. A Rho-  
7 actin signaling pathway shapes cell wall boundaries in Arabidopsis xylem vessels. Nat.  
8 Commun. 10: 468. DOI: 10.1038/s41467-019-08396-7
- 9 Sugiyama Y, Wakazaki M, Toyooka K, Fukuda H, Oda Y. 2017. A novel plasma membrane-  
10 anchored protein regulates xylem cell-wall deposition through microtubule-dependent lateral  
11 inhibition of Rho GTPase domains. Curr. Biol. 27: 2522-2528.e4.  
12 DOI: 10.1016/j.cub.2017.06.059
- 13 Sulbarán B, Toriz G, Allan GG, Pollack GH, Delgado E. 2014. The dynamic development of  
14 exclusion zones on cellulosic surfaces. Cellulose 21: 1143--1148. DOI: 10.1007/s10570-014-  
15 0165-y
- 16 Sun Q, Sun Y, Juzenas K. 2017. Immunogold scanning electron microscopy can reveal the  
17 polysaccharide architecture of xylem cell walls. J. Exp. Bot. 68: 2231--2244.  
18 DOI: 10.1093/jxb/erx103
- 19 Thompson WP. 1918. Independent evolution of vessels in *Gnetales* and angiosperms. Bot. Gaz.  
20 65: 83--90. DOI: 10.1086/332191

- 1 Tixier A, Herbette S, Jansen S, Capron M, Tordjeman P, Cochard H, Badel E. 2014. Modelling  
2 the mechanical behaviour of pit membranes in bordered pits with respect to cavitation resistance  
3 in angiosperms. *Ann. Bot.* 114: 325--334. DOI: 10.1093/aob/mcu109
- 4 Torres-Ruiz JM, Cochard H, Choat B, Jansen S, López R, Tomášková I, Padilla-Díaz CM, Badel  
5 E, Burlett R, King A, Lenoir N, Martin-StPaul NK, Delzon S. 2017. Xylem resistance to  
6 embolism: presenting a simple diagnostic test for the open vessel artefact. *New Phytol.* 215: 489-  
7 -499. DOI: 10.1111/nph.14589
- 8 Tschernitz JL, Sachs IB. 1975. Observations on microfibril organization of Douglas-Fir bordered  
9 pit-pair membranes by scanning electron microscopy. *Wood and Fiber Sci.* 6: 332--340.
- 10 Tyree MT, Sperry JS. 1989. Vulnerability of xylem to cavitation and embolism. *Annu. Rev.*  
11 *Plant Physiol. Plant Mol. Biol.* 40: 19--36. DOI: 10.1146/annurev.pp.40.060189.000315
- 12 Uehara K, Hogetsu T. 1993. Arrangement of cortical microtubules during formation of bordered  
13 pit in the tracheids of *Taxus*. *Protoplasma* 172: 145--153. DOI: 10.1007/BF01379372
- 14 Vallabh R, Banks-Lee P, Seyam A-F. 2010. New approach for determining tortuosity in fibrous  
15 porous media. *JEFF* 5: 7--15. DOI: 10.1177/155892501000500302
- 16 Vallabh R, Ducoste J, Seyam A-F, Banks-Lee P. 2011. Modeling tortuosity in thin fibrous  
17 porous media using computational fluid dynamics. *J Porous Media* 14: 791--804.  
18 DOI: 10.1615/JPorMedia.v14.i9.40
- 19 Wardrop AB. 1958. The organization of the primary wall in differentiating conifer tracheids.  
20 *Aust. J. Bot.* 6: 299--305. DOI: 10.1071/bt9580299

- 1 Weber F, Koller G, Schennach R, Bernt I, Eckhart R. 2013. The surface charge of regenerated  
2 cellulose fibres. *Cellulose* 20: 2719--2729. DOI: 10.1007/s10570-013-0047-8
- 3 Wheeler E. 1981. Intervascular pitting in *Fraxinus americana* L. *IAWA Bull. n.s.* 2: 169--174.  
4 DOI: 10.1163/22941932-90000726
- 5 Wheeler EA. 1983. Intervascular pit membranes in *Ulmus* and *Celtis* native to the United States.  
6 *IAWA J.* 4: 79--88. DOI: 10.1163/22941932-90000400
- 7 Wheeler JK, Sperry JS, Hacke UG, Hoang N. 2005. Inter-vessel pitting and cavitation in woody  
8 *Rosaceae* and other vesselled plants: a basis for a safety versus efficiency trade-off in xylem  
9 transport. *Plant Cell Environ.* 28: 800--812. DOI: 10.1111/j.1365-3040.2005.01330.x
- 10 Wheeler TD, Stroock AD. 2008. The transpiration of water at negative pressures in a synthetic  
11 tree. *Nature* 455: 208--212. DOI: 10.1038/nature07226
- 12 Williamson VG, Milburn JA. 2017. Xylem vessel length and distribution: does analysis method  
13 matter? A study using *Acacia*. *Aust. J. Bot.* 65: 292--303. DOI: 10.1071/BT16220
- 14 Xu P, Donaldson LA, Gergely ZR, Staehelin LA. 2006. Dual-axis electron tomography: a new  
15 approach for investigating the spatial organization of wood cellulose microfibrils. *Wood Sci.*  
16 *Technol.* 41: 101. DOI: 10.1007/s00226-006-0088-3
- 17 Yang KC. 1978. Fine structure of pits in yellow birch (*Betula alleghaniensis* Britton). *IAWA*  
18 *Bull. n.s.* 4: 71--77.
- 19 Yata S, Itoh T, Kishima T. 1970. Formation of perforation plates and bordered pits in  
20 differentiating vessel elements. *Wood Res.* 50: 1--11.

- 1 Zhang Y, Klepsch M, Jansen S. 2017. Bordered pits in xylem of vesselless angiosperms and their  
2 possible misinterpretation as perforation plates. *Plant Cell Environ.* 40: 2133--2146.  
3 DOI: 10.1111/pce.13014
- 4 Zhang Y, Carmesin C, Kaack L, Klepsch MM, Kotowska M, Matei T, Schenk HJ, Weber M, ,  
5 Walter P, Schmidt V, Jansen S. 2019. High porosity with tiny pore constrictions and unbending  
6 pathways characterise the 3D structure of intervessel pit membranes in angiosperm xylem. *Plant*  
7 *Cell Environ.* DOI: 10.1111/pce.13654.
- 8 Zhang H, Zhao C, Li Z, Li J. 2016. The fiber charge measurement depending on the poly-  
9 DADMAC accessibility to cellulose fibers. *Cellulose* 23: 163--173.
- 10 Zimmermann MH, Brown CL. 1971. *Trees: Structure and Function*. Springer Verlag, New York,  
11 Berlin, Heidelberg.
- 12 Zimmermann MH. 1983. *Xylem Structure and the Ascent of Sap*. Springer Verlag, New York.
- 13 Zwieniecki MA, Melcher PJ, Michele Holbrook NM. 2001. Hydrogel control of xylem hydraulic  
14 resistance in plants. *Science* 291: 1059--1062. DOI: 10.1126/science.1057175
- 15



**Table1:** Literature overview on the chemical compounds in immature and mature intervessel pit membranes, excluding the annulus ring. Signals for hemicellulose and pectins are first grouped together and then listed separately for chemical subclasses. The numbers refer to the references below. An additional character to a numbered reference indicates that different methods or antibodies were used in the same study. CLSM = confocal laser scanning microscopy; FLM = fluorescence light microscopy; TEM = transmission electron microscopy; SEM = scanning electron microscopy; SINS = Scattering scanning near-field optical microscopy combined with ultra-broadband synchrotron infrared radiation and atomic force microscopy infrared nanospectroscopy; PM = pit membrane; ‘+’ = positive signal; ‘++’ strongly positive signal; ‘-’ = negative signal; signals between brackets represent mixed results for the species tested; n.d. = no data. <sup>[1]</sup> (Pereira et al. 2018) *Populus nigra*; <sup>[2]</sup> (Klepsch et al. 2016) *Acer campestre*, *A. monspessulanum*, *A. palmatum*, *A. sataricum*, *A. sieboldianum*; <sup>[3]</sup> (Herbette et al. 2015) *P. tremula* × *P. alba*; <sup>[4]</sup> (Plavcová & Hacke 2011) *Betula papyrifera*, *P. balsamifera*, *Prunus virginiana*, *Amelanchier alnifolia*; <sup>[5]</sup> (Kim et al. 2012) *P. tremula* × *P. tremuloides*; <sup>[6]</sup> (Kim & Daniel 2013) *P. tremula*, *P. tremula* × *P. tremuloides*; <sup>[7]</sup> (Schmid & Machado 1968) *Amburana acreana*, *Bauhinia forficata*, *Goniorhachis marginata*, *Plathymenia foliolosa*, *P. reticulata*; <sup>[8]</sup> (Sun et al. 2017) *Vitis vinifera*, *V. arizonica*, 12 week old samples considered as immature pit membranes; <sup>[9]</sup> (Bamber 1961) *Cryptocarya glaucescens*, *Elaeocarpus grandis*, *Eucalyptus viminalis*, *E. pilularis*, *E. microcorys*, *Flindersia schottiana*, *Sloanea woollsii*, *Sterculia acerijolia*, *Toona australis*; (Schenk et al. 2017<sup>[10]</sup>, 2018<sup>[11]</sup>), *Amphilophium buccinatorium*,

- 1 *Encelia farinosa*, *Geijera parviflora*, *Liriodendron tulipifera*, *Triadica sebifera*; <sup>[12]</sup> (Ruel et al.  
 2 2012) *Arabidopsis thaliana* (WS-0).

3

Chemical substance	Signal		Analytical technique
	immature PM	mature PM	
<b>Cellulose</b>	<sup>+</sup> <sub>[3a,3b]</sub>	<sup>++</sup> <sub>[1,3a,11,12a]</sub> , <sup>+</sup> <sub>[3b,12b]</sub>	SINS <sup>[1]</sup> ; CBM3a <sup>[3a,12a]</sup> , CBM28 <sup>[3b,12b]</sup> antibody TEM <sup>[3,12]</sup> , Direct Red 23 CLSM <sup>[11]</sup>
<b>Hemicellulose</b>	<sup>-</sup> <sub>[3,8]</sub> , <sup>++</sup> <sub>[5,8]</sub>	( <sup>+</sup> ) <sup>[4]</sup> , <sup>-</sup> <sub>[2,3,5,6]</sub>	immunohistochemistry TEM <sup>[3,4,5,6]</sup> , SEM <sup>[8]</sup> , FLM <sup>[2]</sup>
Xyloglucan	<sup>-</sup> <sub>[3]</sub>	( <sup>+</sup> ) <sup>[4]</sup> , <sup>-</sup> <sub>[3,6]</sub>	LM15 antibody TEM <sup>[3,4,6]</sup>
Fucosylated xyloglucan	<sup>++</sup> <sub>[8]</sub>	n.d.	CCRC-M1 antibody SEM <sup>[8]</sup>
Xylan	<sup>++</sup> <sub>[5]</sub> , <sup>-</sup> <sub>[3,8]</sub>	<sup>-</sup> <sub>[2,5]</sub> , <sup>-</sup> <sub>[3]</sub>	LM11 <sup>[2,5]</sup> , AX1 <sup>[3]</sup> antibody TEM and FLM; CCRC-M140 <sup>[8]</sup> antibody SEM
Mannans	<sup>-</sup> <sub>[3]</sub>	<sup>-</sup> <sub>[3]</sub>	LM21 antibody TEM <sup>[3]</sup>
<b>Pectic polysaccharides</b>	<sup>++</sup> <sub>[3,6,8]</sub>	<sup>+</sup> <sub>[1]</sub> , <sup>-</sup> <sub>[2,3,4,6,7]</sub> , ( <sup>+</sup> ) <sup>[4]</sup>	SINS <sup>[1]</sup> ; immunohistochemistry

			TEM <sup>[2,3,4,6]</sup> ; FeCl <sub>3</sub> treatment TEM <sup>[7]</sup>
Homogalacturonan	++ <sup>[3a,3b,6a,6b,8]</sup>	- <sup>[2,3a,3b,4,6a,6b]</sup>	LM18 <sup>[2]</sup> , 2F4 <sup>[3a]</sup> , LM20 <sup>[3,6a]</sup> , JIM5 <sup>[4,8]</sup> , JIM7 <sup>[4]</sup> , LM19 <sup>[6b]</sup> antibody TEM and FLM; JIM5 <sup>[8]</sup> antibody SEM
Rhamnogalacturonan	++ <sup>[3]</sup>	(+) <sup>[4]</sup> , - <sup>[3]</sup>	RU1 <sup>[3]</sup> , LM6 <sup>[4]</sup> antibody TEM
<b>Phenolic compounds</b>	n.d.	++ <sup>[1]</sup>	SINS <sup>[1]</sup>
<b>Lignin</b>	- <sup>[3a, 3b, 3c]</sup>	++ <sup>[1]</sup> , ++ <sup>[3b,3c]</sup> , - <sup>[3a,7,9]</sup>	SINS <sup>[1]</sup> ; Anti-G <sup>[3a]</sup> = condensed lignin, Anti- GS <sup>[3b]</sup> and Anti-S <sup>[3c]</sup> = non- condensed lignin antibody TEM, safranin and fast green staining LM <sup>[7,9]</sup>
<b>Proteins</b>	n.d.	+ <sup>[1a]</sup> , - <sup>[1b]</sup> , (++ <sup>[11]</sup> )	Amide II signal <sup>[1a]</sup> Amide III <sup>[1b]</sup> SINS; NanoOrange CLSM unclear whether inside pit membrane <sup>[11]</sup>
<b>Lipids</b>	n.d.	++ <sup>[10,11]</sup>	OsO <sub>4</sub> contrast TEM, FM1- 43 CLSM

## Figures

**Fig. 1.** Ptychographic X-ray computed tomography (PXCT) measured at the cSAXS beamline (Swiss Light Source, PSI, Switzerland) of an air-dried intervessel wall of *Cinnamomum camphora* at cryogenic conditions in the OMNY instrument (Holler et al. 2018). -- **A, B**) Single slice through the tomographic reconstructions. The maximum gray values on the sample edges are likely caused by gallium contamination of the FIB sample preparation. A slice through a non-rigid tomographic reconstruction using an iterative approach with more details in contrast and reduced radiation damage is shown in B (Odstreil et al. 2019). -- **C**) 3D rendered intervessel wall, showing bordered pits, pit membranes (left) and an uneven inner conduit wall (right), dimensions:  $x = 5.35 \mu\text{m}$ ,  $y = 15.39 \mu\text{m}$ ,  $z = 17.72 \mu\text{m}$ . -- **D**) 3D rendered negative of the central bordered pit pair shown in C, dimensions:  $x = 6.04 \mu\text{m}$ ,  $y = 6.53 \mu\text{m}$ ,  $z = 8.41 \mu\text{m}$ . -- **A** = aperture; -- **PB** = pit border; -- **PC** = pit chamber; -- **VL** = vessel lumen; -- arrow = aspirated and shrunken pit membrane. -- Measurement settings: sample to detector distance 5.212 m, projections 600 in 2 sub-tomograms, using equally spaced angular intervals of  $0.6^\circ$  between  $0^\circ$  to  $180^\circ$  with a  $30 \mu\text{m} * 16 \mu\text{m}$  ( $x * y$ ) field of view. The scan positions in a projection followed a Fermat spiral trajectory with a stepsize of 0.9 micrometers and an exposure time of 25 ms point. The X-ray energy was defined by a Si double crystal monochromator to 6.2 keV. The ptychography and tomography reconstruction followed the recipe akin to Odstreil et al. (2019). FIB-SEM preparation of the sample was performed at the FIB Centre of Ulm University, Germany.

**Fig. 2.** Transverse sections of intervessel pit membranes (**A-D, F**) and a developing perforation plate (**E**) in *Laurus nobilis*. **A-C**) TEM images of developing pit membranes (PM) in root xylem; -- **A**) before hydrolysis, with cytoplasm (CP) inside the pit chambers (PC); -- **B**) hydrolysed on

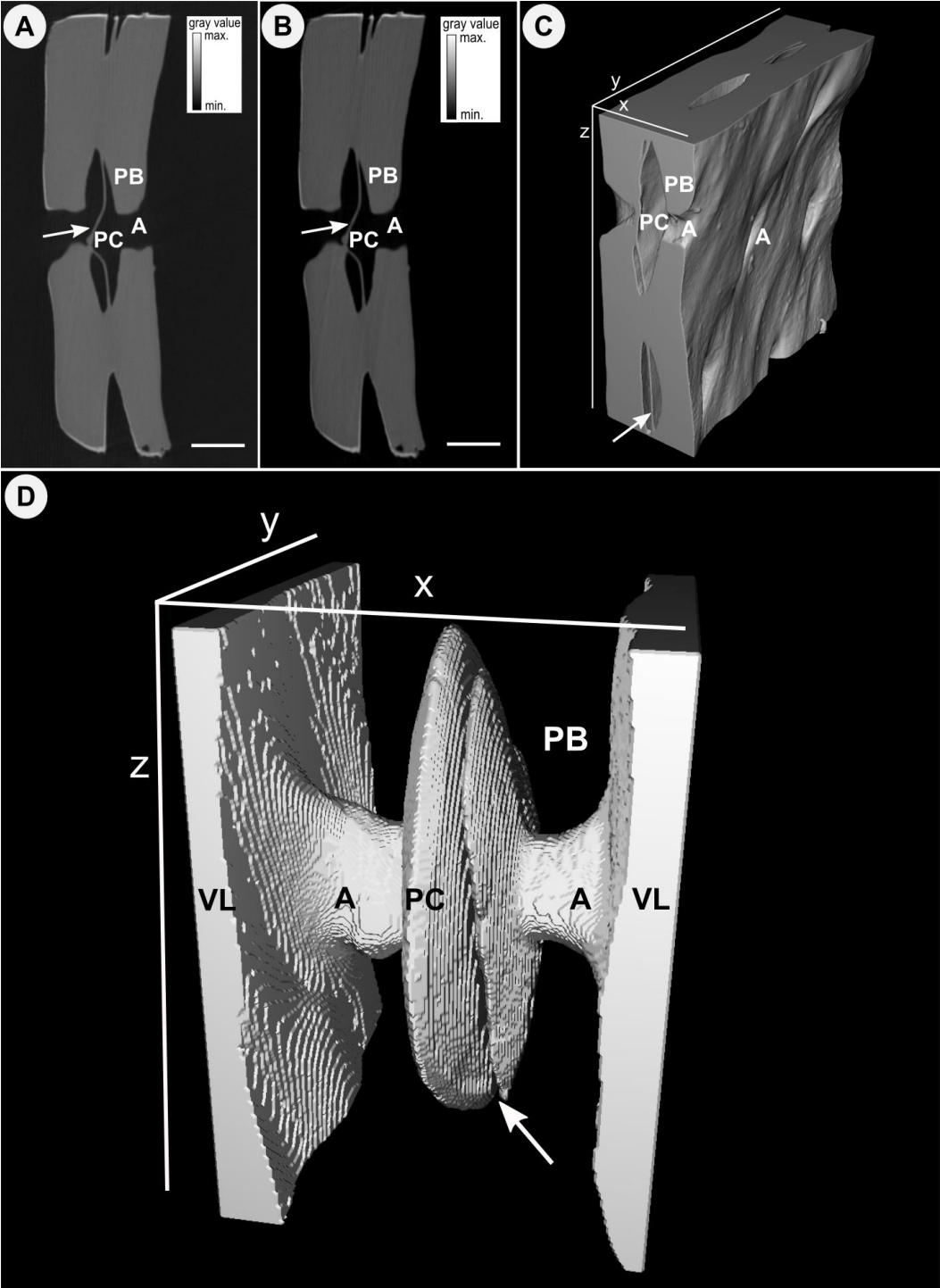
1 the right side; -- C) fully hydrolysed. Note the change in density and thickness of the pit  
 2 membrane (two-headed arrow) as well as the dark lining on the pit chamber walls (arrows). -- E)  
 3 Immature perforation plate (black arrowheads), with a bright appearance, except for the middle  
 4 lamella. -- D) Light microscopy image of a fresh, untreated 3  $\mu\text{m}$  thick section showing thick pit  
 5 membranes (white arrowheads). -- F) Confocal laser scanning microscopy, blue indicates  
 6 autofluorescence of lignin, yellow shows signal for the FM1-43 dye, demonstrating amphiphilic  
 7 lipids on inner vessel walls and in bordered pits. The central black structures represent pit  
 8 membranes (white arrowheads), outlined by amphiphilic lipids. -- CP = cytoplasm; -- CW = cell  
 9 wall; -- PB = pit border; -- PC = pit chamber; -- PM = pit membrane; -- VC = vacuole. -- Scale  
 10 bars in A-C = 0.5  $\mu\text{m}$ ; scale bars in D and F = 5  $\mu\text{m}$ ; scale bar in E = 4  $\mu\text{m}$ .

11 **Fig. 3.** TEM images of transverse sections of mature intervessel pit membranes of *Amphilophium*  
 12 *buccinatorium*, all fixated with glutaraldehyde. -- A) No post-fixation with  $\text{OsO}_4$ , no contrast  
 13 enhancement. -- B) Without  $\text{OsO}_4$  post-fixation, but contrast enhancement with uranyl acetate  
 14 and lead citrate. -- C) Post fixation with  $\text{OsO}_4$ , no contrast enhancement. -- D)  $\text{OsO}_4$  post-fixation  
 15 combined with uranyl acetate treatment. Note the highly invisible pit membrane in A and B, but  
 16 substantial black lining (arrows) of the pit chamber walls and grainy appearance of the pit  
 17 membranes in C and D. -- A = aperture; -- PB = pit border; -- PC = pit chamber; -- PM = pit  
 18 membrane (two-headed arrow); -- scale bars = 500 nm.

19 **Fig. 4.** Drawing of three hydraulically effective pore paths (light grey) through an intervessel pit  
 20 membrane (black colour): -- a) Traditional view of a perfectly straight pore with no pore  
 21 constrictions and equal diameter across the entire pit membrane; -- b) A realistic pore with seven  
 22 pore constrictions (red areas) in a relatively thick pit membrane; -- c) Similar as in b, but with  
 23 four pore constrictions in a pit membrane that is half as thick as in b.

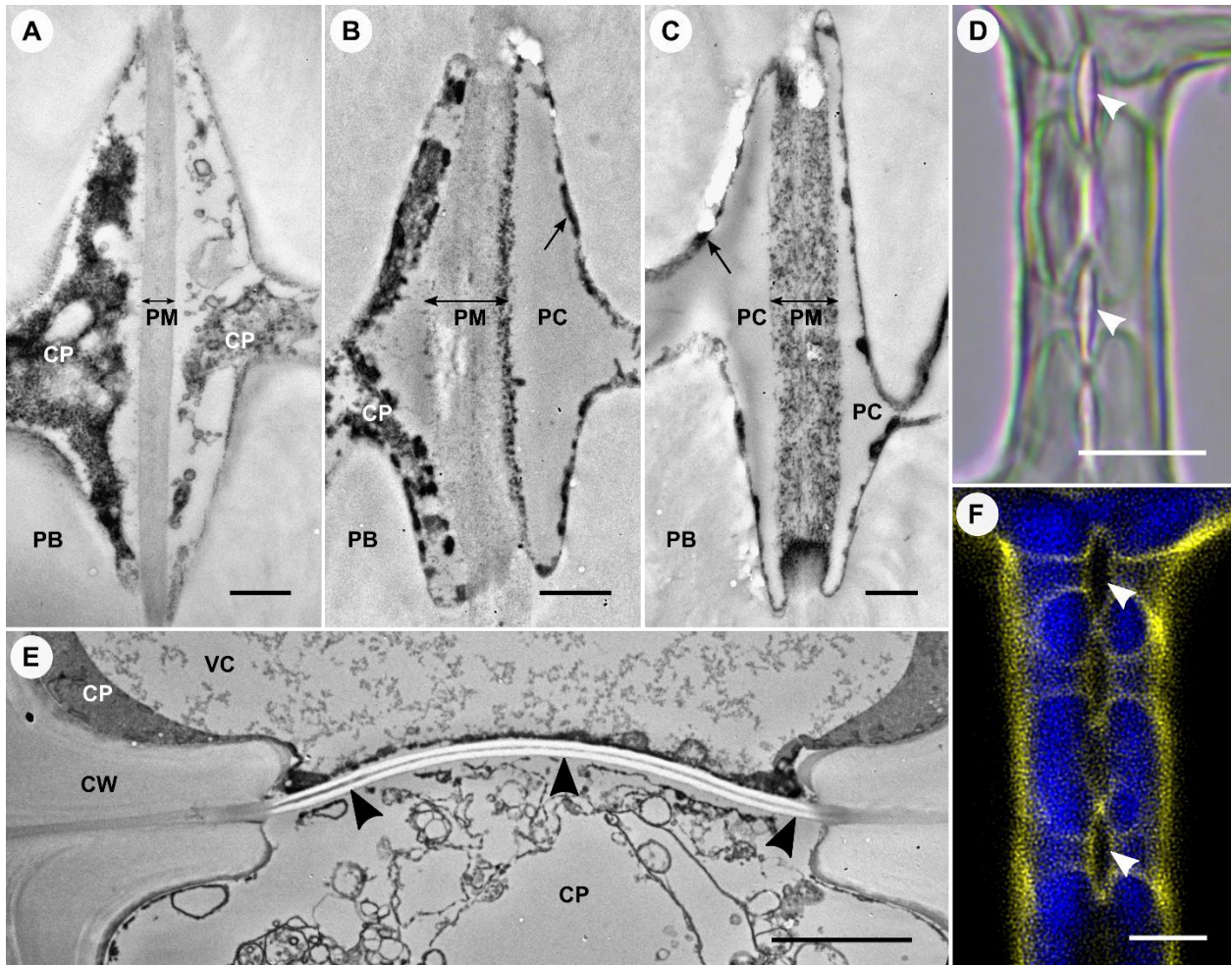
**Fig. 5.** Pore constriction size plotted as a function of air-seeding pressure based on the Young-Laplace equation ( $\Delta P = \kappa \gamma \cos(\alpha) / R$ ). Xylem pressures corresponding to initiation of air-seeding are in the range of -0.4 to -2 MPa (Bartlett et al. 2016), and indicated in blue. Based on modelling and experiments, pore constrictions are found to be about 20 nm (arrow and dashed, vertical line), which are in agreement with air-seeding pressures indicated in blue for the blue line, i.e.  $\kappa = 0.5$  and  $\gamma = 25$  mN/m. An increase in  $\kappa$  and/or  $\gamma$ , shown by the red and black lines, would imply unrealistic, very large pore constrictions to obtain air-seeding pressures within the blue range. -- contact angle  $\alpha = 0$ ; -- pore shape correction factor  $\kappa = 0.5$  (Schenk et al. 2015) or 1, --  $\gamma = 25$  mN/m (the equilibrium surface tension of xylem sap lipids) or 72 mN/m (the surface tension of pure water).

1    **Fig 1:**



2

3

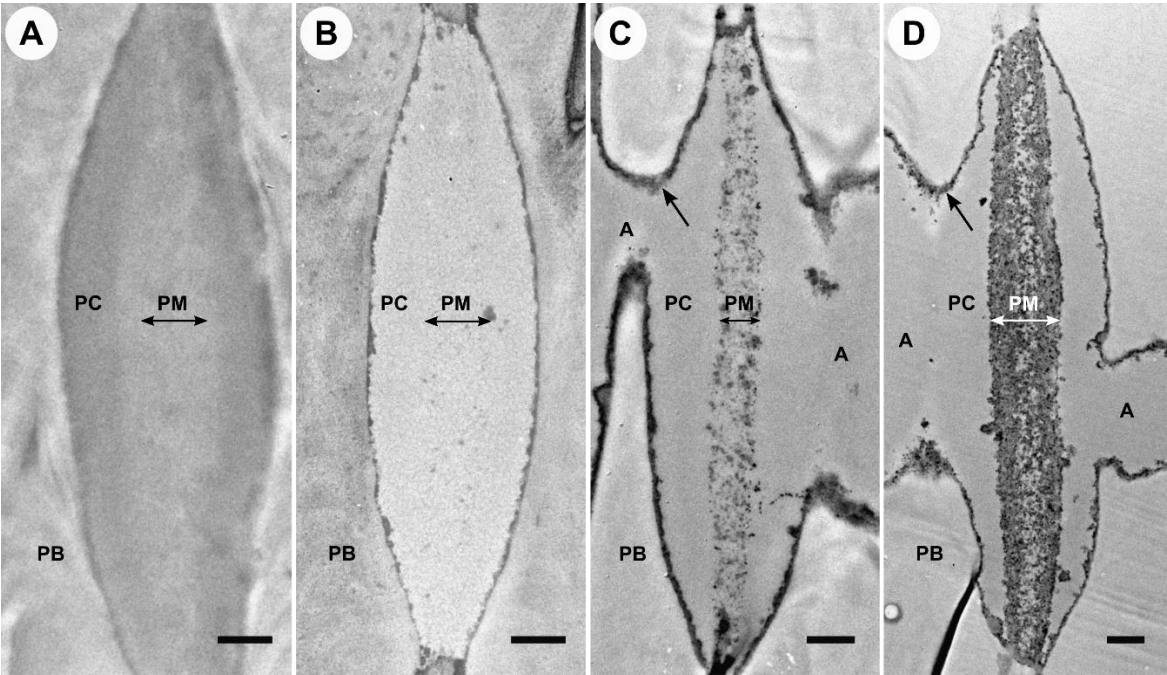
1 **Fig. 2:**

2

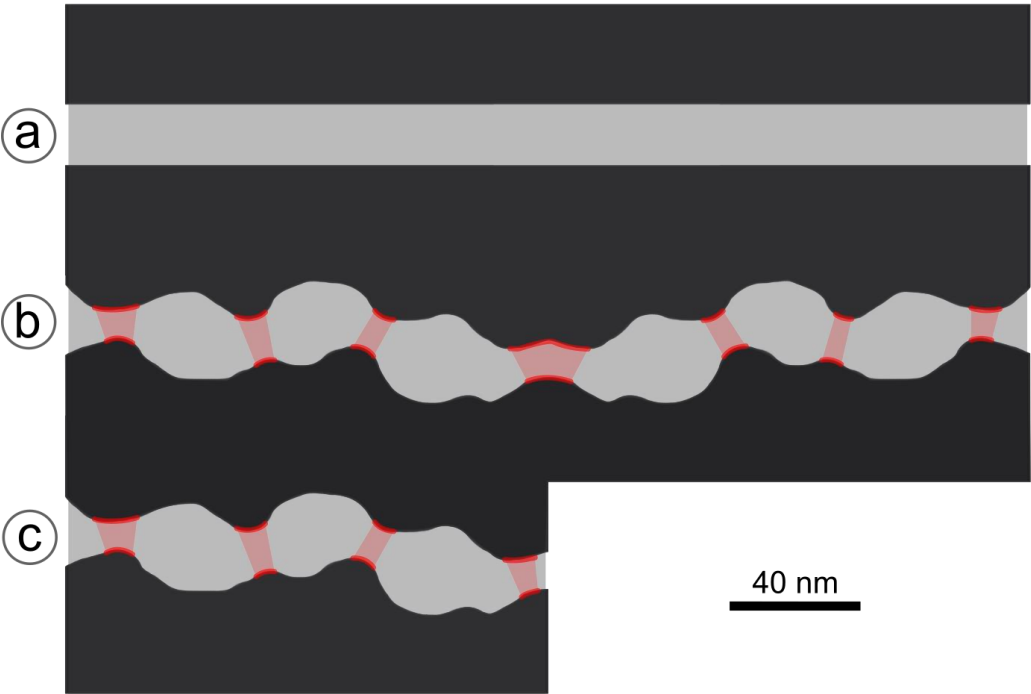
3

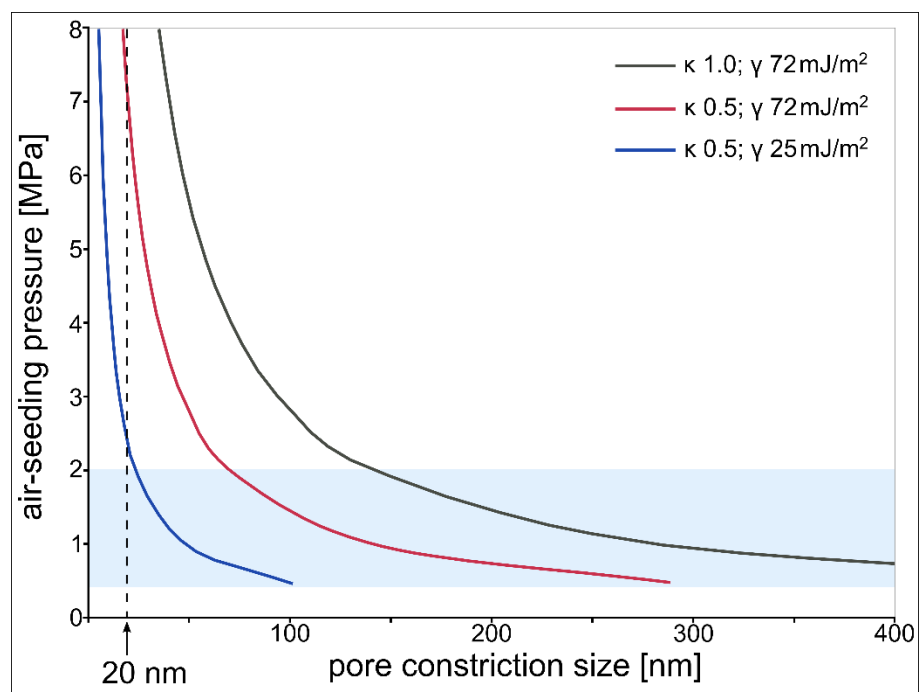


1 **Fig. 3:**



3 **Fig. 4:**



1 **Fig. 5:**

2